Structural Properties and Dynamics of Five-Coordinate Nickel(II)−π-Allyl Complexes Containing Monodentate Phosphorus Ligands

Anna Rufińska, Richard Goddard, Claudia Weidenthaler, Michael Bühl, and Klaus-Richard Pörschke*

Max-Planck-Institut für Kohlenforschung, D-45466 Mülheim an der Ruhr, Germany

Received February 23, 2006

The novel ionic pentacoordinate Ni^{II}−π-allyl complexes [(η^3-C_3H_5)Ni(PMe_3)$_3$]Y (**1a**−**d**) and [(η^3-C_3H_5)Ni{P(OMe)$_3$}$_3$]Y (**2a**−**d**) (Y = SO_3CF_3 (**a**), PF_6 (**b**), Br (**c**), I (**d**)) have been synthesized and investigated by DSC, solid-state NMR, and X-ray single-crystal and powder diffractometry. Apart from **1a**, all complexes are polymorphic. The PMe_3 complexes **1b**−**d** undergo monoclinic-monoclinic phase transitions. The solid-state structures of **1a** and **1b-II** are rigid at low temperature but fluxional at ambient temperature, whereas those of **1c-II** and **1d-II** are almost rigid, while somewhat faster dynamics occur for **1c-I** and **1d-I**. Similarly, the structures of **2c-II** and **2d-II** are fully or almost fully rigid at ambient temperature. The properties of the P(OMe)$_3$-ligated OTf and PF_6 salts **2a**,**b** are completely different. **2a** crystallizes in the triclinic phase **2a-II**, which transforms at −21 °C into the highly mobile, plastically crystalline mesophase **2a-I** with a cubic primitive cell. **2b** crystallizes from solution in the monoclinic phase **2b-III**, having a rigid structure, and transforms at ambient temperature reversibly into the similarly crystalline phase **2b-II**, which undergoes slow dynamics. Heating either phase to 53 °C gives rise to the plastically crystalline mesophase **2b-I**. For complexes **1a**−**d** (all phases) and the phases **2a-II** and **2b-II** the solid-state dynamics start with turnstile rotation of the three phosphorus ligands. For the mesophases **2a-I** and **2b-I** additional π-allyl ligand mobility has been established and anion mobility must also be assumed. DFT MO calculations on the cations **1** and **2** and the parent PH_3 complex **3** gave low rotational barriers of up to 3.5 kcal/mol in the gas phase. Complexes **2a**,**b** are rare examples of metallorganic plastic crystals (dynamically disordered mesophases).

Introduction

π-Allyl rotation and π−σ allyl isomerization are the most important fluxional processes that metal−π-allyl complexes undergo.[1] In asymmetric catalysis the occurrence of these dynamics can determine the stereochemical outcome of the reaction.[2] Generally it is true to say, however, that *all* metal−π-allyl complexes with nonbridging π-allyl ligands undergo at least one of these processes if the temperature is high enough. The processes can be distinguished by NMR, provided that the difference in the activation energies of the individual rearrangements is sufficiently large. Since in many cases the activation energy of π−σ allyl isomerization is lower than that of π-allyl rotation, the latter is more difficult to detect. Typical examples of well-studied π-allyl rotations are given in Table 1.[3]

There has been some controversy as to whether facile π-allyl rotation is feasible for M^{II}−π-allyl complexes (M = Ni, Pd, Pt). The homoleptic, formally square-planar complexes M(η^3-C_3H_5)$_2$ (M = Ni, Pd, Pt)[4] exist in solution as trans/cis mixtures in slow equilibrium. The interchange of the isomers has been followed by magnetization transfer techniques,[1d,5] and the activation energies of both π-allyl rotation and π−σ allyl rearrangement for the M(η^3-C_3H_5)$_2$ complexes can be estimated to be in the range of 25 kcal/mol. Nevertheless, for all complexes *trans*-/*cis*-M(η^3-C_3H_5)$_2$ π-allyl rotation occurs at a lower temperature (between −30 and 0 °C) and is thus preferred over π−σ allyl rearrangement (>0 °C).[1d] No detailed mechanistic information on these isomerizations is known thus far.

* To whom correspondence should be addressed. E-mail: poerschke@mpi-muelheim.mpg.de.

(1) (a) Vrieze, K. In *Dynamic Nuclear Magnetic Resonance Spectroscopy*; Jackman, L. M., Cotton, F. A., Eds.; Academic: New York, 1975; pp 441−487. (b) Mann, B. E. In *Comprehensive Organometallic Chemistry*; Wilkinson, G., Ed.; Pergamon: Oxford, England, 1982; Vol. 3, Chapter 20, pp 110−111. (c) Faller, J. W. *Adv. Organomet. Chem.* **1978**, *16*, 211. (d) Benn, R. Habilitationsschrift, Universität Siegen, Germany, 1984.

(2) Pfaltz, A.; Lautens, M. In *Comprehensive Asymmetric Catalysis*; Springer: Berlin, Heidelberg, Germany, 1999; pp 833−884.

(3) (a) Becconsall, J. K.; O'Brien, S. *Chem. Commun.* **1966**, 720. (b) Davison, A.; Rode, W. C. *Inorg. Chem.* **1967**, *6*, 2124. Faller, J. W.; Incorvia, M. J. *Inorg. Chem.* **1968**, *7*, 840. (c) Nesmeyanov, A. N.; Ustynyuk, Y. A.; Kritskaya, I. I.; Shchembelov, G. A. *J. Organomet. Chem.* **1968**, *14*, 395. (d) Trofimenko, S. *J. Am. Chem. Soc.* **1968**, *90*, 4754. (e) Powell, J.; Shaw, B. L. *J. Chem. Soc. A* **1968**, 583. (f) Holloway, C. E.; Kelly, J. D.; Stiddard, M. H. B. *J. Chem. Soc. A* **1969**, 931. (g) Cooke, M.; Goodfellow, R. J.; Green, M.; Parker, G. *J. Chem. Soc. A* **1971**, 16. (h) Faller, J. W.; Chen, C.-C.; Mattina, M. J.; Jakubowski, A. *J. Organomet. Chem.* **1973**, *52*, 361. (i) Faller, J. W.; Haitko, D. A. *J. Organomet. Chem.* **1978**, *149*, C19. (j) Faller, J. W.; Adams, M. A. *J. Organomet. Chem.* **1979**, *170*, 71. (k) Benn, R.; Rufinska, A.; Schroth, G. *J. Organomet. Chem.* **1981**, *217*, 91. (l) Baker, P. K.; Clamp, S.; Connelly, N. G.; Murray, M.; Sheridan, J. B. *J. Chem. Soc., Dalton Trans.* **1986**, 459. (m) Mann, B. E.; Shaw, S. D. *J. Organomet. Chem.* **1987**, *326*, C13.

(4) Wilke, G.; Bogdanovic, B. *Angew. Chem.* **1961**, *73*, 756. Wilke, G. *Angew. Chem.* **1963**, *75*, 10; *Angew. Chem., Int. Ed. Engl.* **1963**, *2*, 105. Wilke, G.; Bogdanovic, B.; Hardt, P.; Heimbach, P.; Keim, W.; Kröner, M.; Oberkirch, W.; Tanaka, K.; Steinrücke, E.; Walter, D.; Zimmermann, H. *Angew. Chem.* **1966**, *78*, 157; *Angew. Chem., Int. Ed. Engl.* **1966**, *5*, 151. Bönnemann, H.; Bogdanovic, B.; Wilke, G. *Angew. Chem.* **1967**, *77*, 817; *Angew. Chem., Int. Ed. Engl.* **1967**, *6*, 804. Jolly, P. W.; Wilke, G. In *The Organic Chemistry of Nickel*; Academic Press: New York, London, 1974; Vol. 1, p 345. Wilke, G. (Studiengesellschaft Kohle mbH) Ger. Patent 1,194,417, 1965. Wilke, G. (Studiengesellschaft Kohle mbH) U.S. Patent 3,468,921, 1969.

(5) (a) Becconsall, J. K.; O'Brien, S. *J. Organomet. Chem.* **1967**, *9*, P27. (b) O'Brien, S. *J. Chem. Soc. A* **1970**, 9.

10.1021/om0601807 CCC: $33.50
Publication on Web 03/30/2006

Table 1. Examples of M−η^3-C_3H_5 Complexes with Established π-Allyl Rotation

compd	chem phenomenon	detection method[a]	ref
$CpMo(\eta^3\text{-}C_3H_5)(CO)_2$	interchange between endo and exo isomers	NMR	3b
$(indenyl)Mo(\eta^3\text{-}C_3H_5)(CO)_2$	interchange between endo and exo isomers	NMR	3h
$CpMo((1,2,7\text{-}\eta^3)\text{-}3\text{-Me-benzyl})(CO)_2$	interchange between endo and exo isomers	MT	3m
$H_2B(pz)_2Mo(CO)_2(\eta^3\text{-}C_3H_5)$	racemization; syn-syn, anti-anti proton exchange of asym bound π-allyl ligand	NMR	3d
$[(\eta^3\text{-}C_3H_5)M(CO)_3(P\text{-}P)]PF_6$ (M = Mo, W)	racemization; syn-syn, anti-anti proton exchange of asym bound π-allyl ligand	NMR	3i
$(CO)_4W(\eta^3\text{-}C_3H_5)X$ (X = Br, I)	interchange between isomers		3f
$M_2(\eta^3\text{-}C_3H_5)_4$ (M = Cr, Mo)	interchange between isomers	MT	3k
$(\eta^3\text{-}C_3H_5)Fe(CO)_3X$	interchange between endo and exo isomers	MT	3c,j
$(\eta^3\text{-}C_3H_5)_2Fe(CO)_2$	equilibration of inequivalent allyl ligands, $E \approx 4.6$ kcal/mol[3e]	NMR	3c
$(\eta^3\text{-}C_3H_5)_2Ru(CO)_2$	racemization; syn-syn, anti-anti proton exchange of asym bound π-allyl ligands	NMR	3g
$[(\eta^3\text{-}C_3H_5)Fe(L)(NO)_2]PF_6$	racemization; syn-syn, anti-anti proton exchange of asym bound π-allyl ligands	MT	3l
$Co(\eta^3\text{-}C_3H_5)_3$	partial or full equilibration of allyl ligands	MT	1d
$Rh(\eta^3\text{-}C_3H_5)_3$	partial equilibration of allyl ligands	NMR	3a
$LRh(\eta^3\text{-}C_3H_5)_2Cl$	syn-syn, anti-anti proton exchange of one allyl ligand	NMR	3e
$M(\eta^3\text{-}C_3H_5)_2$ (M = Ni, Pd, Pt)	interchange between trans and cis isomers	MT	1d, 5

[a] Legend: NMR, line-shape analysis of solution NMR; MT, magnetization transfer techniques.

For square-planar (*SP*-4) Pd−π-allyl complexes containing coligands, an apparent rotation of the π-allyl group relative to the other ligands is a frequently encountered phenomenon. However, it has been shown that for complexes with monodentate[6a] or particular chelating nitrogen coligands[6b,c] such a process is initiated by cleavage of a Pd−N bond and generation of a tricoordinate intermediate, while for complexes with other coligands formation of a stereochemically nonrigid five-coordinate intermediate has been invoked (considering the allyl ligand to occupy two coordination sites).[7] The occurrence of π-allyl rotation has also been suggested for *SP*-4 Ni−π-allyl complexes, but without compelling evidence.[8]

Since stereochemical nonrigidity represents an inherent property of five-coordinated transition-metal complexes,[9] π-allyl rotation can be expected to occur more readily for five-coordinate than for four-coordinate M^{II}−π-allyl complexes. Although a number of neutral or ionic five-coordinate 18e Ni^{II}−allyl complexes have been reported, examples of which include $(\eta^3\text{-allyl})Ni(Ph_2PC_2H_4PPh_2)Br$,[10a,b] $(\eta^3\text{-}C_3H_5)Ni\{P(OPh)_3\}_2X$ (X = halide, $O_3SC_6H_4Me$),[10c] $(\eta^3\text{-}C_3H_5)Ni(pz_3BH)$,[11a] $(\eta^3\text{-}C_3H_5)Ni(pz'_3BH)$,[11b] $[(\eta^3\text{-}C_3H_5)Ni\{PhP(C_2H_4PPh_2)_2\}]BPh_4$,[11c] and $[(\eta^3\text{-}C_3H_5)Ni(SbPh_3)_3]BAr'_4$,[11d] no information is available on the structural dynamics of the complexes. Fluxional structures *in solution* have been suggested for nonisolated, thermally labile $(\eta^3\text{-allyl})Ni(diphos)Ar$ complexes, but without details being given.[12a] Carmona et al. noted a dynamic structure for $(\eta^3\text{-}C_3H_4Me)Ni(Me_2PC_2H_4PMe_2)Cl$[12b] but did not discuss the dynamics in depth. $\pi-\sigma$ allyl isomerization was reported for the cyanide complexes $(\eta^3\text{-}C_3H_5)Ni(PEt_3)_2CN$[13a] and $(\eta^3\text{-}C_3H_5)Ni(dippe)CN$.[13b] The isolated $[(\eta^3\text{-}syn\text{-}C_3H_4Me)Ni\{P(OEt)_3\}_3]PF_6$ was impure, and related nonisolated products were characterized by NMR.[14] Some examples of isolated five-coordinate Pd^{II}−π-allyl and Pt^{II}−π-allyl complexes such as $[(\eta^3\text{-}C_3H_5)Pd(C_{10}H_{14}S_4)]OTf$[15a] (OTf = trifluoromethanesulfonate, O_3SCF_3), $(\eta^3\text{-}C_3H_3Me_2)Pd(C_{12}H_6N_2Me_2)Cl$,[15b] and $(\eta^3\text{-}C_3H_5)Pt(PPh_3)_2Cl$[16] are also known.

A series of five-coordinate isoelectronic neutral $(\eta^3\text{-allyl})ML_3$ (M = Co, Rh, Ir; L = e.g. phosphine, phosphite) complexes have also been studied. Seminal studies on the structure and dynamic properties of $(\eta^3\text{-}C_3H_5)Co\{P(OMe)_3\}_3$ and its derivatives[17] have been carried out by Muetterties et al., while $(\eta^3$-

(6) (a) Faller, J. W.; Incorvia, M. J.; Thomsen, M. E. *J. Am. Chem. Soc.* **1969**, *91*, 518. (b) Albinati, A.; Kunz, R. W.; Ammann, C. J.; Pregosin, P. S. *Organometallics* **1991**, *10*, 1800. (c) Gogoll, A.; Örnebro, J.; Grennberg, H.; Bäckvall, J.-E. *J. Am. Chem. Soc.* **1994**, *116*, 3631.

(7) (a) Vrieze, K.; Maclean, C.; Cossee, P.; Hilbers, C. W. *Recl. Trav. Chim. Pays-Bas* **1966**, 1077. (b) Vrieze, K.; Cossee, P.; Hilbers, C. W.; Praat, A. P. *Recl. Trav. Chim. Pays-Bas* **1967**, 769. (c) Vrieze, K.; Cossee, P.; Praat, A. P.; Hilbers, C. W. *J. Organomet. Chem.* **1968**, *11*, 353. (d) Faller, J. W.; Incorvia, M. J. *J. Organomet. Chem.* **1969**, *19*, P13. (e) van Leeuwen, P. W. N. M.; Praat, A. P. *J. Organomet. Chem.* **1970**, *21*, 501. (f) Crociani, B.; Di Bianca, F.; Giovenco, A.; Boschi, T. *Inorg. Chim. Acta* **1987**, *127*, 169. (g) Crociani, B.; Antonaroli, S.; Paci, M.; Di Bianca, F.; Canovese, L. *Organometallics* **1997**, *16*, 384.

(8) For discussions on the operation of the π-allyl rotation mechanism in Ni^{II}−allyl complexes, see: (a) Hampton, P. D.; Wu, S.; Alam, T. M.; Claverie, J. P. *Organometallics* **1994**, *13*, 2066. (b) Aresta, M.; Quaranta, E.; Dibenedetto, A.; Giannoccaro, P.; Tommasi, I.; Lanfranchi, M.; Tiripicchio, A. *Organometallics* **1997**, *16*, 834. Aresta, M.; Dibenedetto, A.; Quaranta, E.; Lanfranchi, M.; Tiripicchio, A. *Organometallics* **2000**, *19*, 4199.

(9) (a) Eaton, D. R. *J. Am. Chem. Soc.* **1968**, *90*, 4272. (b) Orioli, P. L. *Coord. Chem. Rev.* **1971**, *6*, 285. (c) Wood, J. S. *Prog. Inorg. Chem.* **1972**, *16*, 227. (d) Morassi, R.; Bertini, I.; Sacconi, L. *Coord. Chem. Rev.* **1973**, *11*, 343. (e) Rossi, A. R.; Hoffmann, R. *Inorg. Chem.* **1975**, *14*, 365. (f) Demuynck, J.; Strich, A.; Veillard, A. *Nouv. J. Chim.* **1977**, *1*, 217. (g) Anderson, G. K.; Cross, R. J. *Chem. Soc. Rev.* **1980**, *9*, 185. (h) Holmes, R. R. *Prog. Inorg. Chem.* **1984**, *32*, 119. (i) Cross, R. J. *Chem. Soc. Rev.* **1985**, *14*, 197. (j) Auf der Heyde, T. P. E.; Bürgi, H.-B. *Inorg. Chem.* **1989**, *28*, 3982. (k) Aullón, G.; Alvarez, S. *Inorg. Chem.* **1996**, *35*, 3137.

(10) (a) Hegedus, L. S.; Corey, E. J. Unpublished work. Churchill, M. R.; O'Brien, T. A. *Chem. Commun.* **1968**, 246; *J. Chem. Soc. A* **1970**, 206. (b) Cameron, T. S.; Prout, C. K. *Acta Crystallogr., Sect. B* **1972**, *28*, 2021. (c) Taube, R.; Gehrke, J.-P. *J. Organomet. Chem.* **1987**, *327*, 419.

(11) (a) Lehmkuhl, H.; Näser, J.; Mehler, G.; Keil, F.; Danowski, F.; Benn, R.; Mynott, R.; Schroth, G.; Gabor, B.; Krüger, C.; Betz, P. *Chem. Ber.* **1991**, *124*, 441. (b) Shirasawa, N.; Nguyet, T. T.; Hikichi, S.; Moro-oka, Y.; Akita, M. *Organometallics* **2001**, *20*, 3582. (c) Clegg, W.; Cropper, G.; Henderson, R. A.; Strong, C.; Parkinson, B. *Organometallics* **2001**, *20*, 2579. (d) Jiménez-Tenorio, M.; Puerta, M. C.; Salcedo, I.; Valerga, P.; Costa, S. I.; Gomes, P. T.; Mereiter, K. *J. Chem. Soc., Chem. Commun.* **2003**, 1168.

(12) (a) Kurosawa, H.; Ohnishi, H.; Emoto, M.; Chatani, N.; Kawasaki, Y.; Murai, S.; Ikeda, I. *Organometallics* **1990**, *9*, 3038. (b) Carmona, E.; Palma, P.; Poveda, M. L. *Polyhedron* **1990**, *9*, 757.

(13) (a) Walter, D.; Wilke, G. *Angew. Chem.* **1966**, *78*, 941; *Angew. Chem., Int. Ed. Engl.* **1966**, *5*, 897. (b) Brunkan, N. M.; Jones, W. D. *J. Organomet. Chem.* **2003**, *683*, 77.

(14) (a) Tolman, C. A. *J. Am. Chem. Soc.* **1970**, *92*, 6777. Tolman, C. A. *J. Am. Chem. Soc.* **1970**, *92*, 6785. (b) For an early treatise on $[(\pi\text{-allyl})NiL_3]^+$ complexes, see: Jolly, P. W.; Wilke, G. *The Organic Chemistry of Nickel*; Academic: New York, 1974; Vol. 1, p 364.

(15) (a) Liu, S.; Lucas, C. R.; Newlands, M. J.; Charland, J.-P. *Inorg. Chem.* **1990**, *29*, 4380. (b) Hansson, S.; Norrby, P.-O.; Sjögren, M. P. T.; Åkermark, B.; Cucciolito, M. E.; Giordano, F.; Vitagliano, A. *Organometallics* **1993**, *12*, 4940.

(16) (a) Volger, H. C.; Vrieze, K. *J. Organomet. Chem.* **1966**, *6*, 297. (b) Baird, M. C.; Wilkinson, G. *J. Chem. Soc. A* **1967**, 865.

Scheme 1

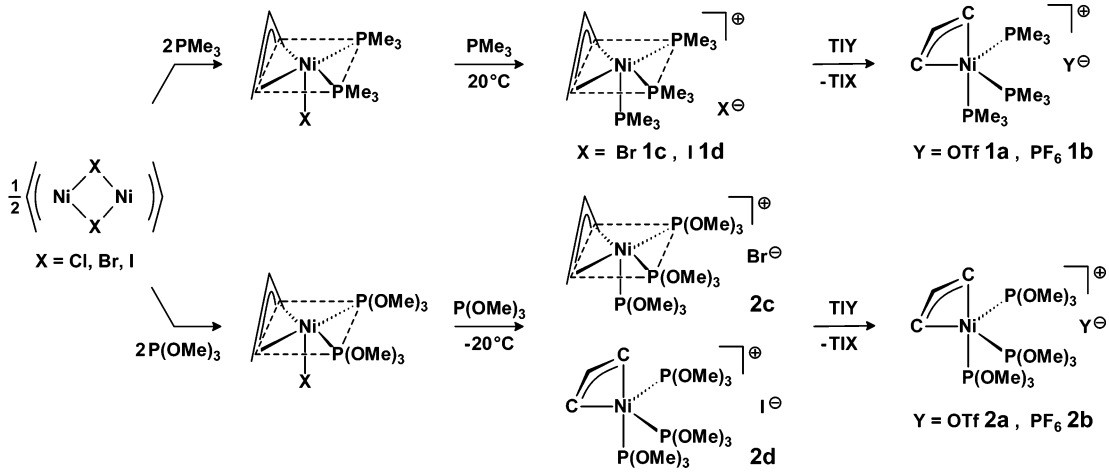

C_3H_5)Rh{$P(OMe)_3$}$_3$[18] and various (η^3-allyl)IrL_3[19] complexes have been less extensively investigated.

In view of the presently slim evidence of π-allyl rotation in Ni^{II}−allyl complexes we have undertaken a comprehensive study of the dynamic properties of such species. So far we have synthesized and structurally characterized ionic five-coordinate [(η^3-C_3H_4R)NiL_3]Y (R = H, Me) complexes containing uniform monodentate donor ligands L (L = phosphine, phosphite) by DSC, solution and solid-state NMR, X-ray single-crystal and powder diffractometry, and DFT calculations. In this paper we focus on [(η^3-C_3H_5)Ni(PMe_3)$_3$]Y and [(η^3-C_3H_5)Ni{$P(OMe)_3$}$_3$]Y complexes with Y = OTf, PF_6, Br, I.[20]

Results

I. Synthesis and Solution Properties of [(η^3-C_3H_5)Ni(PMe_3)$_3$]Y (1a−d) and [(η^3-C_3H_5)Ni{$P(OMe)_3$}$_3$]Y (2a−d). Reaction of {(η^3-C_3H_5)Ni(μ-X)}$_2$ (X = Br, I) with 3 equiv of PMe_3 or $P(OMe)_3$ per Ni affords the five-coordinate Ni^{II}−π-allyl halides **1c**,**d** and **2c**,**d**. The syntheses of **1c**,**d** are best done in THF, in which they are insoluble, so that the red microcrystals precipitate. Complex **2c** is soluble in diethyl ether, from which it forms large orange cubes, while the likewise orange cubes of **2d** crystallize from a CH_2Cl_2/Et_2O mixture (Scheme 1). The syntheses pass through (η^3-C_3H_5)NiL_2X intermediates (L = PMe_3, $P(OMe)_3$), of which (η^3-C_3H_5)Ni{$P(OMe)_3$}$_2$Br has been isolated as large red-brown needles and [(η^3-C_3H_5)Ni{$P(OMe)_3$}$_2$]-PF_6 as yellow plates. Reacting the ionic **1c**,**d** and **2c**,**d** with TlOTf or $TlPF_6$ in CH_2Cl_2 results in halide replacement and formation of the OTf and PF_6 salts **1a** (red cubes), **1b** (small orange-brown crystals), **2a** (large orange columns), and **2b** (fine orange needles). The latter complexes are also prepared in one-pot reactions by reacting any of the halides {(η^3-C_3H_5)Ni(μ-X)}$_2$ (X = Cl, Br, I)) with the stoichiometric amounts of PMe_3 or $P(OMe)_3$ and TlOTf or $TlPF_6$. The synthesis of the PMe_3 complexes **1a**−**d** can be carried out at ambient temperature, although the complexes slowly decompose in solution at this temperature. For the synthesis of the $P(OMe)_3$ derivatives **2a**−**d** the temperature must be kept at −20 °C to avoid a degradation reaction of the $P(OMe)_3$ ligands by allylation.

As far as the thermal stability of the solids is concerned, the PMe_3 complexes of the OTf and PF_6 salts **1a**,**b** seem indefinitely stable at ambient temperature, whereas the red halides **1c**,**d** turn brown over the course of several days. We will show below that solid **1b**−**d** are polymorphic and undergo reversible crystalline−crystalline transitions.

The $P(OMe)_3$ complex **2a** is also stable at ambient temperature, and here it unexpectedly is present in a plastically crystalline mesophase, **2a-I** (see below).[21] Complex **2b** crystallizes from THF solution at 0 °C in its crystalline low-temperature phase **2b-III**. Solid-state NMR (see below) has shown that the well-formed orange crystals of **2b-III** transform at 20−35 °C into the likewise crystalline red phase **2b-II**. Storage between −20 and 10 °C converts **2b-II** back into **2b-III**. The transformation is thus reversible, with a phase-transition temperature of about 15 °C (eq 1). When the transition **2b-II** → **2b-III** is

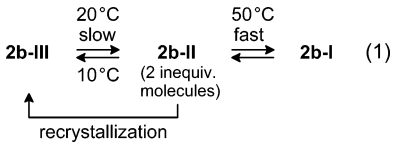

started at low temperature (e.g., −20 °C), it is rather slow and might come to a halt, but it can be continued at a higher temperature, where it again might stop, and it eventually proceeds to completion at 10 °C. There appears to be an induction period for each restart.[22] We further note that the rate of the transitions slows down with each cycle, presumably due to a loss of homogeneity of the crystal. Nevertheless, even after a series of transformations it has been possible to revert all

(17) (a) Muetterties, E. L.; Hirsekorn, F. J. *J. Am. Chem. Soc.* **1973**, *95*, 5419. Muetterties, E. L.; Hirsekorn, F. J. *J. Am. Chem. Soc.* **1974**, *96*, 7920. (b) Rakowski, M. C.; Hirsekorn, F. J.; Stuhl, L. S.; Muetterties, E. L. *Inorg. Chem.* **1976**, *15*, 2379. (c) Thompson, M. R.; Day, V. W.; Tau, K. D.; Muetterties, E. L. *Inorg. Chem.* **1981**, *20*, 1237. (d) Bleeke, J. R.; Burch, R. R.; Coulman, C. L.; Schardt, B. C. *Inorg. Chem.* **1981**, *20*, 1316. (e) Bleeke, J. R.; Peng, W.-J. *Organometallics* **1984**, *3*, 1422. Bleeke, J. R.; Peng, W.-J. *Organometallics* **1986**, *5*, 635. (f) Sernau, V.; Huttner, G.; Scherer, J.; Zsolnai, L.; Seitz, T. *Chem. Ber.* **1995**, *128*, 193.

(18) Bottrill, M.; Green, M. *J. Organomet. Chem.* **1976**, *111*, C6.

(19) (a) Merola, J. S.; Kacmarcik, R. T.; Van Engen, D. *J. Am. Chem. Soc.* **1986**, *108*, 329. (b) Bleeke, J. R.; Haile, T.; New, P. R.; Chiang, M. Y. *Organometallics* **1993**, *12*, 517. Bleeke, J. R.; Luaders, S. T.; Robinson, K. D. *Organometallics* **1994**, *13*, 1592.

(20) (a) The results have been partially presented at the ACS National Meetings in Boston, MA, August 18−22, 2002, Anaheim, CA, March 28-April 1, 2004, and San Diego, CA, March 13−17, 2004: Pörschke, K.-R.; Jonas, K. *Abstr. Pap.-Am. Chem. Soc.* **2002**, *224*, INOR-009. Pörschke, K.-R.; Goddard, R.; Rufińska, A.; Bühl, M. *Abstr. Pap.-Am. Chem. Soc.* **2004**, *227*, INOR-463. Pörschke, K.-R.; Rufińska, A.; Goddard, R.; Weidenthaler, C. *Abstr. Pap.-Am. Chem. Soc.* **2005**, *229*, INOR-813. (b) Part II: Rufińska, A.; Goddard, R.; Pörschke, K.-R. Manuscript in preparation.

(21) By convention, the solid phases of the compounds are designated **I**, **II**, ... in the order of decreasing temperature starting from the melting (decomposition) point.

Table 2. Solution NMR Data of the Allyl Group of [(η³-C_3H_5)Ni(PMe_3)$_3$]OTf (1a) and [(η³-C_3H_5)Ni{$P(OMe)_3$}$_3$]OTf (2a)

	δ(H)			δ(C)		
	H1	H2/4	H3/5	C2	C1/3	Δδ(C)
1a[a]	5.15	3.01	1.92	91.2	56.9 (q)	34.3
2a[b]	5.29	3.71	2.67	95.1	61.8 (q)	33.3

[a] Temperature −80 °C. J(H2/4,H1) = 5.4 Hz, J(H3/5,H1) = 11.0 Hz, J(P,H3/5) = 4.9 Hz; J(PC) = 4.5 Hz. PMe_3 ligand: δ(H) 1.27, δ(C) 17.4 (∑J(PC) = 31 Hz), δ(P) −14.1. [b] Temperature −30 °C. J(H2/4,H1) = 6.5 Hz, J(H3/5,H1) = 11.9 Hz, J(P,H3/5) = 3.9 Hz; J(PC) = 6.8 Hz. $P(OMe)_3$ ligand: δ(H) 3.63(m), δ(C) 52.6(d), δ(P) 139.7.

samples of **2b-II** into **2b-III** by storing them at 10 °C for several days. We also show below that **2b** forms the plastically crystalline phase **2b-I** at higher temperature. Recrystallization of any phase from solution leads to recovery of pristine **2b-III**.

The bromide **2c** decomposes at ambient temperature in the course of several days to give a red oil, while the somewhat more stable iodide **2d** becomes brown and sticky after 2 weeks. When they are heated quickly, **1a**−**d** and **2a**,**b** display melting/decomposition points in the range of 120−140 °C, whereas **2c**,**d** transform into viscous oils at about 50 and >65 °C, respectively (see section III, DSC).

The ambient-temperature IR spectra of the solid complexes **1a**−**d** and **2a**−**d** are inconspicuous, and in the ESI+ mass spectra, after cleavage of one of the ligands L, the cations [(η³-C_3H_5)NiL_2]$^+$ are observed as base ions.

Solution NMR Spectra. The solution ^{1}H and ^{13}C NMR spectra of **1a**−**d** are best resolved at −80 °C and those of **2a**−**d** at −30 °C. The spectra of the respective cations of **1a**−**d** and **2a**−**d** are virtually identical. The chemical shifts as determined for **1a** and **2a** are given in Table 2. The spectra display for the allyl ligand three somewhat broad resonances for the meso (H1), syn (H2/4), and anti (H3/5) protons (A_2M_2X spin system with additional phosphorus couplings) and two resonances for the central (C2) and terminal carbon atoms (C1/3). The signal of the anti protons H3/5 is a doublet of quartets, and that of C1/3 is a quartet. The couplings show that the complex cations are undissociated and that the three phosphorus atoms are equivalent in solution. All allyl resonances are at higher field for the phosphine complexes **1a**−**d** than for the phosphite derivatives **2a**−**d**. It appears as a characteristic feature of [(η³-C_3H_5)NiL_3]$^+$ complexes (L = phosphorus ligand) that C2 resonates at relatively high field, δ(C) ∼90 (compared to δ(C) >105 for [(η³-C_3H_5)NiL_2]$^+$), resulting in a small shift difference between C2 and C1/3 of Δδ(C) ≈ 33−35 ppm. For **1a**−**d** at −80 °C the PMe_3 ^{1}H signal is a singlet and the ^{13}C signal is a multiplet of eight lines of equal intensity flanked by small satellites, resulting from a higher order spin system. For **2a**−**d** the −30 °C $P(OMe)_3$ ^{1}H signal is an "inverse triplet" and the ^{13}C signal a doublet. The ^{31}P resonance is a sharp singlet down to −80 °C. Considering that all the complexes for which the structures have been determined adopt C_1 point symmetry in the solid state (see below), the low-temperature (LT) solution NMR spectra of **1a**−**d** and **2a**−**d** indicate that fluxionality of the structure occurs by exchange of the terminal allyl methylene groups concomitant with syn-syn, anti-anti exchange of the allyl protons and an equilibration of the three phosphorus ligands. The dynamics are consistent with a rather facile rotation of the three phosphorus atoms relative to the π-allyl ligand.

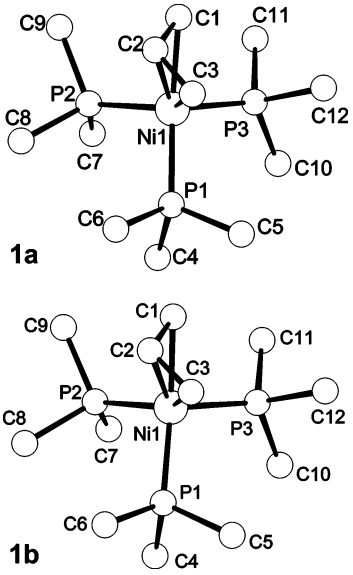

Figure 1. Molecular structures of [(η³-C_3H_5)Ni(PMe_3)$_3$]OTf (**1a**) and [(η³-C_3H_5)Ni(PMe_3)$_3$]PF_6 (**1b**) (only cations depicted). For structural data, see Table 4.

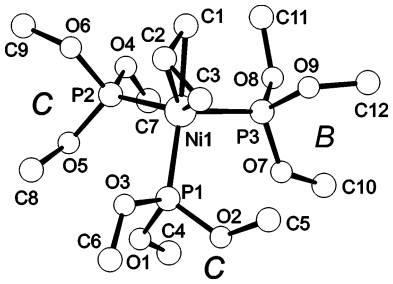

Figure 2. Molecular structure of [(η³-C_3H_5)Ni{$P(OMe)_3$}$_3$]PF_6 (**2b**) (only the cation depicted). For structural data, see Table 4.

At ambient temperature the proton A_2M_2X spin system is maintained, but all phosphorus couplings of the allyl protons and carbon atoms are lost and the allyl resonances are shifted to lower field in the direction of the resonances expected for the corresponding [(η³-C_3H_5)NiL_2]Y complexes. According to the spectra the five-coordinate cations undergo partial PMe_3 and $P(OMe)_3$ ligand dissociation at ambient temperature, whereas π−σ allyl isomerization is still insignificant.

II. Single-Crystal Molecular Structures of 1a,b and 2b−**d.** The structures of the complexes in their crystalline low-temperature phases as obtained from solutions are shown for the PMe_3 complexes **1a**,**b** in Figure 1 and for the $P(OMe)_3$ derivatives **2b**−**d** in Figures 2−4, respectively (only cations depicted). Experimental details and selected structural data are given in Tables 3 and 4, respectively. (Thus far we have not been able to obtain single crystals of **1c**,**d**, **2a**, and **2b-II** suitable for an X-ray crystallographic analysis.)

The complexes **1a**,**b** and **2b**,**d** (Figures 1, 2, and 4) comprise a Ni cation, bearing a π-bound C_3H_5 and three PMe_3 or $P(OMe)_3$ ligands, and a completely separated OTf, PF_6, or I anion. The Ni atoms are formally five-coordinate, assuming the allyl ligand occupies two coordination sites, and the cations adopt geometries which can be considered intermediate between square pyramidal (*SPY*-5) and trigonal bipyramidal (*TBP*-5), but closer to *TBP*-5. C1 of the allyl ligand and P1, which together subtend the largest C−Ni−P angle at Ni (α), can be thought of as occupying the two axial coordination sites of a formal *TBP*-5 structure.

(22) An induction period (incubation time) of crystal nucleation is not unusual and follows from nucleation theory. (a) Rao, C. N. R.; Rao, K. J. *Phase Transitions in Solids*; McGraw-Hill: New York, 1978; p 86. (b) Kelton, K. F. Crystal Nucleation in Liquids and Glasses. In *Solid State Physics*; Ehrenreich, H., Turnbull, D., Eds.; New York: Academic Press: 1991; Vol. 45, pp 75−177.

Table 3. Crystal Data for 1a,b and 2b−d

	1a	1b	2b	2c	2d
empirical formula	$C_{13}H_{32}F_3NiO_3P_3S$	$C_{12}H_{32}F_6NiP_4$	$C_{12}H_{32}F_6NiO_9P_4$	$C_{12}H_{32}BrNiO_9P_3$	$C_{12}H_{32}INiO_9P_3$
color	orange	yellow-orange	yellow	orange-red	orange-yellow
formula wt	477.07	472.97	616.97	551.91	598.90
temp (K)	100	100	100	100	100
wavelength (Å)	0.710 73	0.710 73	0.710 73	0.710 73	0.710 73
cryst syst	triclinic	monoclinic	monoclinic	monoclinic	monoclinic
space group	$P\bar{1}$ (No. 2)	$P2_1/c$ (No. 14)	$P2_1$ (No. 4)	$P2_1$ (No. 4)	$P2_1/n$ (No. 14)
unit cell dimens					
a (Å)	8.7689(12)	10.3078(2)	8.3014(2)	10.7181(2)	11.6045(1)
b (Å)	10.4345(7)	12.9243(2)	11.3832(2)	8.1124(1)	16.1857(3)
c (Å)	12.294(2)	15.9969(3)	12.9936(3)	12.6683(2)	12.2778(2)
α (deg)	89.967(5)	90	90	90	90
β (deg)	76.814(6)	90.1620(10)	92.894(1)	96.078(1)	94.796(1)
γ (deg)	89.988(11)	90	90	90	90
V (Å^3)	1095.2(2)	2131.12(7)	1226.28(5)	1095.31(3)	2298.03(6)
Z	2	4	2	2	4
V/Z (Å^3)	548	533	613	548	575
calcd density (Mg m^{-3})	1.45	1.47	1.67	1.67	1.73
abs coeff (mm^{-1})	1.23	1.25	1.14	2.97	2.43
F(000) (e)	500	984	636	568	1208
cryst size (mm^3)	0.16 × 0.15 × 0.04	0.07 × 0.05 × 0.04	0.28 × 0.28 × 0.06	0.16 × 0.14 × 0.12	0.06 × 0.04 × 0.02
θ range for data collecn (deg)	2.39−33.13	5.10−26.37	4.66−31.04	3.45−30.99	3.02−31.48
index ranges	$-13 \le h \le 9$ $-16 \le k \le 15$ $-16 \le l \le 18$	$-11 \le h \le 12$ $-9 \le k \le 16$ $-19 \le l \le 19$	$-12 \le h \le 12$ $-16 \le k \le 16$ $-18 \le l \le 18$	$-15 \le h \le 15$ $-11 \le k \le 11$ $-18 \le l \le 18$	$-17 \le h \le 17$ $-23 \le k \le 23$ $-18 \le l \le 18$
no. of rflns collected	11 402	11 167	32 634	27 294	47 940
no. of indep rflns	7888 (R_{int} = 0.0412)	4285 (R_{int} = 0.0816)	7752 (R_{int} = 0.0359)	6968 (R_{int} = 0.0843)	7602 (R_{int} = 0.0379)
no. of rflns with $I > 2\sigma(I)$	7008	3091	7480	5606	6606
completeness (%)	94.6 (θ = 33.13°)	98.5 (θ = 26.37°)	99.2 (θ = 31.04°)	99.6 (θ = 30.99°)	99.8 (θ = 31.48°)
abs cor	Gaussian	Gaussian	multiscan	Gaussian	multiscan
max/min transmissn	0.952 32/0.837 09	0.95/0.90	0.9197/1.0	0.750 63/0.632 56	0.9048/1.0
full-matrix least squares	F_o^2	F_o^2	F_o^2	F_o^2	F_o^2
no. of data/restraints/param	7888/0/218	4285/0/262	7757/1/289	6968/1/235	7602/0/235
goodness of fit on F^2	1.044	1.210	1.041	1.028	1.027
final R indices ($I > 2\sigma(I)$)					
R1	0.0424	0.0891	0.0269	0.0496	0.0251
wR2	0.0887	0.1971	0.0691	0.0791	0.0621
R indices (all data)					
R1	0.0527	0.1247	0.0287	0.0721	0.0332
wR2	0.0942	0.2107	0.0701	0.0857	0.0655
abs structure param			0.026(7)	−0.011(8)	
largest diff peak/hole (e Å^{-3})	0.594/−0.897	0.772/−0.626	0.555/−0.412	0.740/−0.549	0.764/−0.713

The C1−Ni−P1 angle falls into the relatively narrow range of 155−157° in the four compounds. The other allyl terminal carbon atom C3 and the phosphorus atoms P2 and P3 consequently occupy the three approximately equatorial sites. The allyl ligand (bite angle C1−Ni−C3 ≈ 70°) therefore spans axial and equatorial sites. The two equatorial phosphorus atoms are, however, inequivalent and the point group of the cations is necessarily C_1.

The angle C3−Ni−P2, defined as the second largest at Ni (β), lies in the range of 135−142° for **1a**,**b** and **2b**,**d**, while the C3−Ni−P3 angle at 101−112° is markedly smaller. It follows from the assignment that P2 is exo and P3 endo to the opening of the allyl ligand. There is no overlap of the three angle ranges. In all four cations the P2−Ni−P3 angle is in the range 108−114° (thus not reaching an ideal 120°), while the angles P1−Ni−P2 and P1−Ni−P3 lie around 100° (instead of the ideal 90°). The bonds to the axially coordinated ligands, Ni−P1 (2.15−2.18 Å) and Ni−C1 (2.06−2.08 Å), are shorter than those to the equatorial ligands, Ni−P2/P3 (2.17−2.24 Å) and Ni−C3 (2.09−2.13 Å). Since Ni−P3 is usually longer than Ni−P2 (for **1a** it is slightly shorter by 0.006(1) Å), one might conclude

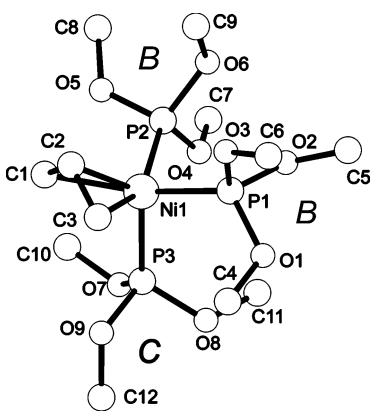

Figure 3. Molecular structure of $[(\eta^3\text{-}C_3H_5)Ni\{P(OMe)_3\}_3]Br$ (**2c**) (only the cation depicted). For structural data, see Table 4.

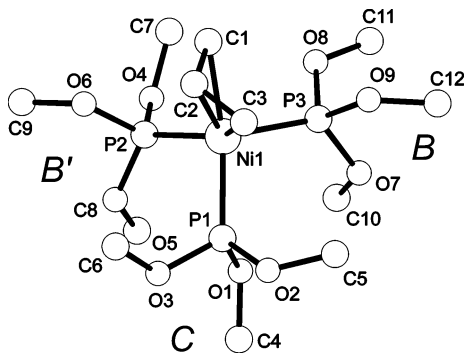

Figure 4. Molecular structure of $[(\eta^3\text{-}C_3H_5)Ni\{P(OMe)_3\}_3]I$ (**2d**) (only the cation depicted). *B′* is intermediate between *B* and *C*. For structural data, see Table 4.

Table 4. Bond Distances (Å), Angles (deg), and the Angular Parameter τ for the Structurally Characterized [(η^3-C_3H_5)NiL_3]Y (L = Phosphorus Ligand) Complexes 1a,b and 2b−d

	1a	1b	2b	2c	2d
Ni1−P1	2.178(1)	2.182(2)	2.1514(5)	2.1507(11)	2.1508(5)
Ni1−P2	2.238(1)	2.226(2)	2.1886(5)	2.1805(11)	2.1786(5)
Ni1−P3	2.232(1)	2.239(3)	2.2149(5)	2.2235(12)	2.2344(5)
Ni1−C1	2.063(2)	2.058(9)	2.081(2)	2.090(4)	2.0773(19)
Ni1−C2	1.997(2)	2.007(9)	2.011(2)	1.998(4)	2.0126(19)
Ni1−C3	2.101(3)	2.090(9)	2.130(2)	2.092(4)	2.1229(19)
C1−C2	1.409(4)	1.402(14)	1.415(3)	1.387(6)	1.408(3)
C2−C3	1.401(4)	1.396(14)	1.399(3)	1.388(6)	1.400(3)
C1−Ni1−C3	69.8(1)	68.8(4)	69.04(8)	68.42(17)	69.74(8)
C1−Ni1−P1 (α)	156.3(1)	155.0(3)	154.92(6)	151.15(13)	157.01(6)
C1−Ni1−P2	96.5(1)	95.5(3)	90.88(6)	93.81(13)	91.98(6)
C1−Ni1−P3	89.3(1)	91.9(3)	93.12(6)	98.33(14)	94.43(6)
C3−Ni1−P1	86.5(1)	87.6(3)	87.72(6)	89.03(13)	91.69(6)
C3−Ni1−P2 (β)	135.3(1)	141.4(4)	138.23(6)	149.80(13)	142.00(6)
C3−Ni1−P3	111.6(1)	107.5(4)	105.23(6)	102.24(13)	101.17(6)
P1−Ni1−P2	99.32(3)	98.22(9)	101.14(2)	97.88(4)	95.10(2)
P1−Ni1−P3	101.44(3)	103.39(10)	102.31(2)	104.07(4)	102.64(2)
P2−Ni1−P3	110.53(3)	108.12(10)	112.33(2)	104.46(4)	113.58(2)
τ	0.35	0.23	0.28	0.02	0.25

that the axial Ni−P1 bonds are the strongest and the equatorial endo Ni−P3 bonds are the weakest of the three Ni−P bonds.

In view of the noteworthy solid-state properties of some of the complexes (see section III) it seems relevant to point out details of the crystal packing. The ionic crystal structures of **1a**,**b** and **2d** are not unusual; in the PMe_3 complexes **1a**,**b** the cations are irregularly surrounded by eight OTf anions (Ni···S = 5.291−8.606 Å) or six PF_6 anions (Ni···P4 = 5.446−7.507 Å), while in the structure of the $P(OMe)_3$ complex **2d** the cations are surrounded by seven iodide ions with a large Ni···I distance range (5.774−9.316 Å).

The single crystals of **2b** obtained from the solvent (phase **III**) belong to the acentric (chiral) space group $P2_1$ (No. 4), and there are two molecules in the unit cell, each with the same chirality. The unit cell volume measured at 100 K (V = 1220.05(7) Å^3) corresponds to 610 Å^3 per ion pair, which is the largest of all the compounds listed in Table 3. Cations and PF_6 anions in the crystal of **2b** are packed such that each is surrounded by eight counterions in a distorted cubic arrangement (Ni1···P4 interionic distances, 6.457(1)−8.378(1) Å). At room temperature the unit cell volume of **2b** increases to V = 1290.16(5) Å^3 (645 Å^3 per molecule), concomitant with markedly larger atomic displacement parameters for all atoms. When a pristine crystal was heated to 310 K, there was a strong reduction in the number of diffracted intensities, though some individual diffraction intensities were still visible. At this temperature the internal consistency of equivalent reflections was poor (R_{int} = 0.43) and no satisfactory refinement was possible. Cooling the same crystal to 100 K resulted in re-formation of an excellent crystal (V = 1226.28(5) Å^3, V/Z = 613 Å), the structure of which could be refined to an R index of 0.0269 (wR2 = 0.070 for 7757 reflections; Tables 3 and 4). In contrast, heating a crystal to 323 K resulted in diffuse scattering with isolated reflections, which remained on cooling the sample to room temperature and then to 0 °C within a period of several hours.

In contrast to the *TBP*-5 structures of **1a**,**b** and **2b**,**d**, the structure of the cation in the bromide salt **2c** is *SPY*-5 (Figure 3). The C1−Ni1−P1 angle (α) is 151.2(1)°, while the C3−Ni1−P2 angle (β) is 149.8(1)°. Thus, these two angles in **2c** are very smilar and correspond to the trans basal angles in a *SPY*-5 structure. Consistent with the basal position of the π-allyl ligand, the Ni1−C1 and Ni1−C3 bonds are almost equal in length (2.091 Å, mean). Of the three P−Ni−P angles in the cation, the angle between the basal phosphorus atoms is the smallest (P1−Ni1−P2 = 97.88(4)°), while the angles between P1 and P2 and the apicial P3 are somewhat larger and are about the same (104.3°, mean). As expected for an apical ligand, the Ni1−P3 distance at 2.2235(12) Å is slightly longer than the Ni1−P1 and Ni1−P2 distances, which do not differ significantly (2.1507(11) and 2.1805(11) Å). It is worth noting that the Ni−P bonds in the $P(OMe)_3$ complexes **2b**−**d** are all shorter than the corresponding bonds in the PMe_3 complexes **1a**,**b**.

Despite the different geometries of the cations, the bromide **2c** crystallizes in the same chiral space group as **2b**, namely $P2_1$, with two identical molecules in the unit cell. In the crystal packing of the ions in **2c** each Ni atom is surrounded distorted octahedrally by six identical bromide ions and each Br anion has six nearest-neighbor cations (Ni1···Br1 distances 5.117(1)−7.820(1) Å). The distortion is such that in a plane of the cations the bromide ions are moved away from their expected central position between the cations, allowing the cations to come closer to each other, while the bromide appears to be embedded in an array of 12 or more OMe substituents of the $P(OMe)_3$ ligands. In particular, one Br^- is preferentially drawn toward one Ni atom (Ni1···Br1 = 5.117(1) Å), resulting in relatively short Br1···C distances to the phosphite methoxy C8 and C9 atoms (3.677(3), 3.840(3) Å) and C1 and C2 of the allyl group (4.107(3), 4.061(3) Å) on the same cation. There is, however, also an additional short contact between Br1 and C10 on a neighboring cation (3.651(4) Å). It is not clear whether the *SPY*-5 geometry of the cation in **2c** is due to direct interactions between the cations and the Br anions or due to the crystal packing.

The structural change at the metal in **2b**−**d** (*TBP*-5 vs *SPY*-5 structure) is accompanied by a conformational change of the methoxy groups in the phosphite ligands (cf. Figures 2−4). The methoxy groups of the $P(OMe)_3$ ligand are rather flexible and can fold up to give a Tolman cone angle[23] as small as 103° or open up to as much as 138°, thereby adjusting to the available space in the complex. Following the notation of ref 24, the conformation with two OMe groups trans and one gauche to Ni is designated *B* (cone angle of 117°) and that with one OMe arm trans and two gauche to Ni is designated *C* (cone angle of 130°). In *TBP*-5 **2b** the conformations of the three $P(OMe)_3$ ligands are *B*,*C*,*C* (average cone angle is 126°) with the endo equatorial (and most distant) $P(OMe)_3$ ligand (P3) having the slim *B* conformation. (The conformation of the $P(OMe)_3$ ligands in the likewise *TBP*-5 **2d** is quite similar.) In **2c** with *SPY*-5 geometry the $P(OMe)_3$ conformations are *B*,*B*,*C* (average cone angle is 121°) and here, as expected, the close to one another and tightly bound basal $P(OMe)_3$ groups (P1, P2) have conformation *B*.

The data show that there is more available space in the *TBP*-5 structure than in the *SPY*-5 structure. The structures of **2b**,**d** suggest that the average cone angle of 126° represents an upper limit for ligands to be coordinated at Ni in a [(η^3-C_3H_5)NiL_3]$^+$ complex. While the complexes are also formed for L = PMe_3 (cone angle 118°), the larger cone angle of PEt_3 (132°) might explain why the derivative with L = PEt_3 has not been observed.

Finally, for a semiquantitative assessment of the geometrical distortions of the five-coordinate structures of **1a**,**b** and **2b**−**d** from ideal *TBP*-5 and *SPY*-5 structures we refer to continuous symmetry measures.[25a] For five-coordinate complexes, two parameters are in common use, and these are the trigonal-bipyramidal symmetry measure *S*(TBP), which describes the

(23) Tolman, C. A. *Chem. Rev.* **1977**, *77*, 313.
(24) Smith, J. M.; Coville, N. J. *Organometallics* **2001**, *20*, 1210.

Table 5. Selected Solid-State CP-MAS NMR Data for [(η^3-C_3H_5)Ni(PMe_3)$_3$]Y (1a−d) and [(η^3-C_3H_5)Ni{$P(OMe)_3$}$_3$]Y (2a−d)

		δ(C)			δ(P)				J(PP) (Hz)		
	T (K)	C2	C1/3	PMe_3	P1	P2	P3	P(1−3)	P1P2	P1P3	P2P3
1a[a]	183	93.4	60.8, 55.7	17.5 ($w_{1/2}$ = 70 Hz)[f]	2.7	−18.2	−25.2	(−13.6)[g]	32	28	132
	301	93.8	58.7	18.5				−16.0			
1b[c]	234	93.1[d]	62.0, 56.0[d]	18.1 (3C), 16.8 (6C)[d]	0.2	−18.5	−26.5	(−14.9)[g]	*h*	*h*	130
	301	93.8	61.1, 57.2	17.8				−16.7			
1c-II	183	94.6[f]	62.6, 61.8[f]	19.3 ($w_{1/2}$ = 200 Hz)[f]	−0.4	−10.1	−24.3	(−11.6)[g]	*h*	*h*	100
1c-I	301	94.9	62.6, 62.1	20.2				−13.5			
1d-II	167	95.1[d]	63.2, 61.0[d]	19.8[d]	−4.4	−6.4	−24.9	(−11.9)[g]	<30	45	72
1d-I	301	95.7	63.2, 61.0	20.4				−13.8			
	361	96.3	63.3, 61.2	20.5				−14.8			

		δ(C)			δ(P)				J(PP) (Hz)		
	T (K)	C2	C1/3	$P(OMe)_3$	P1	P2	P3	P(1−3)	P1P2	P1P3	P2P3
2a-II	194	∼93.0	67−59	56−50	*i*	*i*	*i*				
2a-I[b]	301	95.9	61.6	53.2				138.8			
2b-III[c]	301	93.2	66.6, 60.0	52.6	151.4	138.5	129.8	(139.9)[g]	42	45	211
2b-II[c]	237	95.0[e]	65.8, 62.2[e]	53.5[e]	149.3	136.3	132.4	(139.3)[g]	58	66	228
		93.9[e]	62.2, 61.0[e]	52.6[e]	143.2	140.7	138.2	(140.7)[g]	82	75	222
2b-I	323	96.2	61.7	53.0				138.8			
2c	301	95.4	68.2, 64.6	55.2 (7C), 52.9 (1C), 49.2 (1C)	139.8	138.2	149.9	(142.6)[g]	<30	53	61
2d	301	97.4	67.4, 57.9	54.9	154.1	138.5	127.8	(140.1)[g]	56[f]	<30[f]	202[f]

[a] OTf: δ(C) 122.0, *J*(FC) = 340 Hz. [b] OTf: δ(C) 122.2, *J*(FC) = 324 Hz. [c] PF_6: δ(P) −144.8 ± 0.2, *J*(PF) = 705 ± 4 Hz. [d] Temperature 217 K. [e] Temperature 301 K. An assignment of the resonances to the individual molecules 1 and 2 has not been performed. [f] Temperature 200 K. [g] Calculated mean given in parentheses. [h] *J*(P1P2) > *J*(P1P3), as indicated by the line widths. These unresolved couplings are expected to amount to 10−30 Hz. [i] See text.

distance of a structure from an ideal trigonal bipyramid, and the simpler angular parameter τ, which we shall use in this paper. τ is defined as $(\alpha - \beta)/60$, where α is the largest and β the second largest L−M−L bond angle of the five-coordinate structure.[25b]

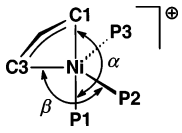

Accordingly, $\tau = 1$ for a perfect *TBP*-5 and $\tau = 0$ for a perfect *SPY*-5 structure, while intermediate structures on the Berry rotation pathway have $0 < \tau < 1$. For π-allyl complexes a further restriction of the magnitude of τ can be imposed by assuming *TBP*-5 geometry with C3 in the equatorial plane, P1 in the axial position, and an allyl group C1−Ni−C3 bite angle of 70°. This limits α, the angle between the two formal axial positions and Ni, to 160° and gives a limiting value of τ = 0.67. Experimentally, for **1a**,**b** and **2b**−**2d** τ is found to be 0.35, 0.23, 0.28, 0.02, and 0.25 respectively (Table 4). The τ value observed for **2c** confirms its almost ideal *SPY*-5 structure. The structures of **1a**,**b** and **2b**,**d** can be classified on the basis of the τ value as lying numerically approximately halfway between *SPY*-5 and *TBP*-5. In fact, comparison of the structures of the various complexes in this work suggests that any τ value >0.1 indicates appreciable *TBP*-5 character.

III. Solid-State Phase Transitions and Structural Dynamics. Further insight into the solid-state properties of the [(η^3-C_3H_5)NiL_3]Y complexes **1a**−**d** and **2a**−**d** was gained by variable temperature (VT) investigations involving Differential Scanning Calorimetry (DSC),[26] X-ray powder diffractometry, and solid state ^{13}C and ^{31}P CP-MAS NMR. Chemical shifts and coupling constants of the latter are listed in Table 5. Examples of all spectra are included in the body of this paper, and additional, similarly illustrative spectra are contained in the Supporting Information (designated in the text with "S"). For introductions into polymorphism,[27] (metallo)mesogens,[28] and the plastically crystalline state,[29] see the given references. In plastic crystals the molecules or ions show a relatively rapid rotational motion on their sites in the lattice.

[(η^3-C_3H_5)Ni(PMe_3)$_3$]Y (Y = OTf (1a), PF_6 (1b)). The well-crystallized PMe_3 triflate complex **1a** shows in the DSC curve only minor endothermic events (80−120 °C) close to the melting point. Due to a starting decomposition of the melt these events cannot be reversed consistently. For the PF_6 salt **1b** (Figure 5) a reversible endothermic λ transition; that is, a change in heat capacity resulting from reorientation of molecular groups is observed at 40.5 °C as a minor event, while melting occurs at 126 °C. Thus, on the basis of the DSC data **1b** appears to form low- and high-temperature phases, **1b-II** and **1b-I**, with a transition temperature of 40.5 °C. The different phases are, however, not reflected in the X-ray powder diffraction spectra, which at 100 K agree perfectly with the spectrum calculated from the single-crystal analysis (monoclinic symmetry) and up to 343 K (70 °C) show only a seemingly continuous and reversible expansion of the elementary cell.

The results from solid-state NMR spectroscopy are in agreement with these findings. In the ambient-temperature (301 K) solid-state ^{31}P CP-MAS NMR spectra complexes **1a**,**b** give rise to single ^{31}P resonances. The spectrum of the triflate **1a** is a sharp singlet ($w_{1/2} \approx 100$ Hz), flanked by a pair of small

(25) (a) Zabrodsky, H.; Peleg, S.; Avnir, D. *J. Am. Chem. Soc.* **1992**, *114*, 7843. (b) Addison, A. W.; Rao, T. N.; Reedijk, J.; van Rijn, J.; Verschoor, G. C. *J. Chem. Soc., Dalton Trans.* **1984**, 1349. Alvarez, S.; Llunell, M. *Dalton Trans.* **2000**, 3288.

(26) Höhne, G. W. H.; Hemminger, W.; Flammersheim, H.-J. *Differential Scanning Calorimetry*, 2nd ed.; Springer: Berlin, 2003.

(27) (a) Fox, D., Labes, M. M., Weissberger, A., Eds. *Physics and Chemistry in the Organic Solid State*; Interscience: New York, 1963−1967; Vols. 1−3. (b) Dunitz, J. D. *Acta Crystallogr., Sect. B* **1995**, *51*, 619. (c) Dunitz, J. D.; Bernstein, J. *Acc. Chem. Res.* **1995**, *28*, 193.

(28) (a) Giroud-Godquin, A.-M.; Maitlis, P. M. *Angew. Chem., Int. Ed.* **1991**, *30*, 375. (b) Serrano, J. L., Ed. *Metallomesogens*; VCH: Weinheim, Germany, 1996. (c) Donnio, B.; Bruce, D. W. *Struct. Bonding* **1999**, *95*, 193.

(29) (a) Timmermans, J. *J. Phys. Chem. Solids* **1961**, *18*, 1. (b) Aston, J. G. In ref 27a, p 543. (c) Gray, G. W.; Winsor, P. A. *Liquid Crystals and Plastic Crystals*; Horwood: Chichester, U.K., 1974; Vols. I and II. (d) Schmid, D.; Wannagat, U. *Chem.-Ztg.* **1974**, *98*, 575. Schmid, D. *Chem.-Ztg.* **1975**, *99*, 12. (e) Sherwood, J. N., Ed. *The Plastically Crystalline State*; Wiley: Chichester, U.K., 1979.

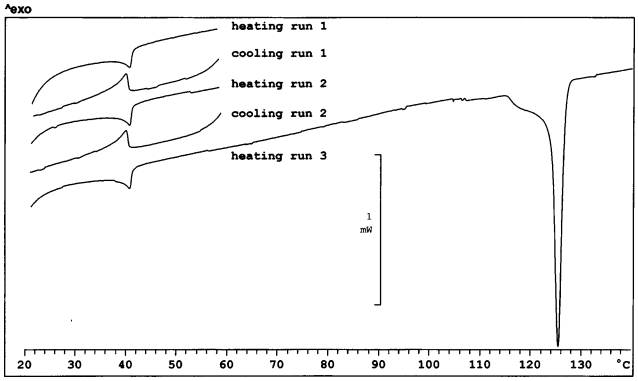

Figure 5. DSC spectrum of $[(\eta^3\text{-}C_3H_5)Ni(PMe_3)_3]PF_6$ (**1b**) at heating and cooling rates of 1 K min^{-1}. DSC was first performed by periodically heating and cooling the sample between 20 and 60 °C. The endothermic λ transition occurs at about 41 °C peak temperature and is reversed at 40 °C, suggesting an actual phase transition temperature of 40.5 °C. Finally, the sample was heated above the melting point (126 °C). The mean enthalpy of transition $\Delta H_{314\ K}$(**II**→**I**) = 1.0 kJ mol^{-1} and entropy of transition $\Delta S_{314\ K}$(**II**→**I**) = 3.2 J K^{-1} mol^{-1} are small compared to the enthalpy and entropy of fusion of $\Delta H_{399\ K}$ = 11.4 kJ mol^{-1} and $\Delta S_{399\ K}$ = 28.6 J K^{-1} mol^{-1}. While the phase transitions in the first part of the spectrum are reversible, after the sample has been heated above the melting point, irreversible spectral effects occur.

(solution NMR type) sidebands (Figure 6). At 234 K the spectrum displays three distinct resonances due to inequivalent PMe_3 ligands, but the fine structure emerges fully only at 183 K. In contrast, at ambient temperature the ^{31}P signal of the cation of **1b-II** (Figure S1) is very broad ($w_{1/2} \approx 1100$ Hz), but it sharpens considerably when the temperature is raised to 313 K ($w_{1/2} \approx 210$ Hz) or 341 K ($w_{1/2} \approx 40$ Hz). The phase change **1b-II** → **1b-I** (313.5 K, DSC) is not visibly associated with a change in the characteristics of the ^{31}P NMR signal. The LT limiting spectrum of **1b-II** with three separate signals is already observed at 234 K, where two resonances have well-resolved *J*(PP) couplings. According to the solid-state VT ^{31}P NMR spectra, complexes **1a**,**b** have rigid structures at low temperature but undergo dynamics of the phosphorus ligands at higher temperatures. The changes in the spectra upon heating are quite similar and are as expected for a continuous enhancement of the rate *k* of the dynamics with coalescence of the resonances. Nevertheless, at a particular temperature the dynamics occur much faster for the triflate **1a** than for the PF_6 salt **1b** (eq 2a).

$$k_{\mathbf{1a}}(\mathrm{OTf}) > k_{\mathbf{1b}}(\mathrm{PF_6}) \qquad (2a)$$

In their limiting LT ^{31}P CP-MAS spectra complexes **1a**,**b** show a low-field pseudo-singlet (unresolved doublet of doublets) at δ(P1) ∼0 and two close high-field doublets of doublets at δ(P2) ∼−18 and δ(P3) ∼−25. The splittings of the latter resonances are due to a large mutual coupling[30] (*J*(P2P3) ≈ 130 Hz) and smaller couplings to P1 (**1a**, *J*(P1P2) = 32 Hz and *J*(P1P3) = 28 Hz). For **1b** the smaller couplings are not resolved but the line width of the resonances indicates that *J*(P1P2) > *J*(P1P3). The large range of chemical shifts, the distribution of signals, and the observed splittings of the signals appear as characteristic features of these compounds. (For a schematic representation of the spectra, see Figure 19.) For both complexes the calculated mean of the chemical shifts of the individual ^{31}P resonances agrees well with the shift of the coalesced resonances and with that in solution.

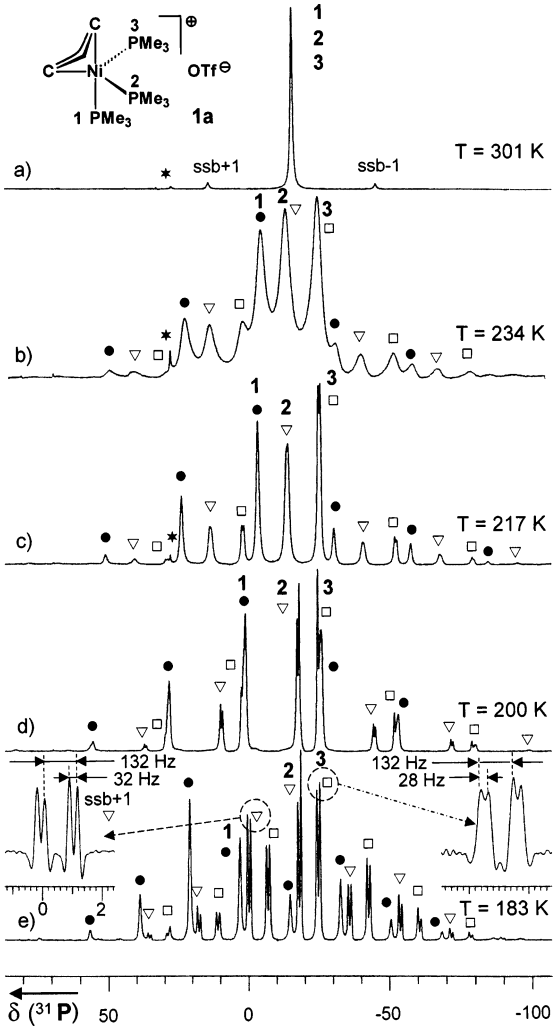

Figure 6. VT ^{31}P CP-MAS NMR spectra of **1a**. The numbers mark the isotropic chemical shifts, while the asterisk marks an impurity. Trace a (301 K, R_0 = 3.6 kHz, 10 s repetition delay): the sharp signal ($w_{1/2}$ = 98 Hz) is flanked by very small first-order spinning sidebands (ssb), similar to a solution spectrum. The spectrum is explained by a fast exchange of the PMe_3 ligands. The half line width depends slightly on the rotational frequency (R_0 = 2.16 kHz, $w_{1/2}$ = 120 Hz; R_0 = 5.8 kHz, $w_{1/2}$ = 83 Hz). Trace b (234 K, R_0 = 3.3 kHz, 4 s repetition delay): three broad singlets (δ(P) −4.8, −13.7, −25.1) and an ssb pattern, typical for solid-state NMR spectra, indicate that the migration of the PMe_3 ligands has slowed significantly. Trace c (217 K, R_0 = 3.3 kHz, 4 s repetition delay): (●) signal of P1 (δ −3.5) and corresponding ssb; (▽) signal of P2 (δ −14.2) and ssb; (□) P3 (δ −25.4) and ssb. Trace d (200 K, R_0 = 3.3 kHz, 4 s repetition delay): the particular rotational frequency of 3300 Hz is close to the chemical shift difference of P1 (δ 1.0) and P3 (δ −25.3), 3200 Hz, resulting in an overlap of the isotropic chemical shifts of these signals with the ssb. The signal of P2 (δ −17.8) is shifted further to high field. Trace e (183 K, R_0 = 2.16 kHz, 3 s repetition delay): the change of chemical shift follows the already observed trend; that is, P1 (δ 2.7) is shifted to lower field and P2 (δ −18.3) to higher field, whereas P3 is unchanged. The inset on the left shows an expansion of ssb + 1 of P2 and the inset on the right an expansion of P3, after Gaussian multiplication prior to Fourier transformation. No splitting is observed for the signal of P1. See also Table 5.

(30) (a) Relatively large couplings *J*(PP) > 100 Hz seem to be characteristic for complexes with high coordination numbers, and such couplings have previously been observed in (η^3-alkenyl)iron tris(phosphite) cations: Ittel, S. D.; Van-Catledge, F. A.; Jesson, J. P. *J. Am. Chem. Soc.* **1979**, *101*, 6905. (b) A large and so far unexplained coupling, *J*(PP) = 150 Hz, has been observed in (η^3-C_3H_4Me)Ni(*cis*-$Ph_2PCH{=}CHPPh_2$)(C_6F_5).[12a]

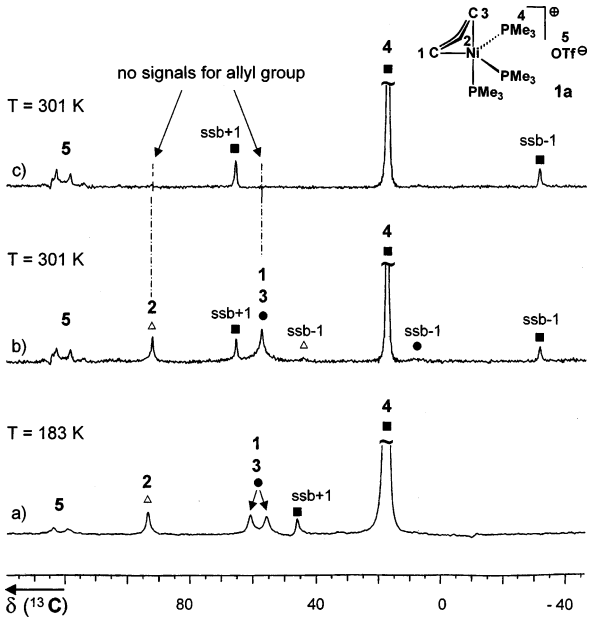

Figure 7. VT ^{13}C CP-MAS NMR spectra of **1a**. For the PMe_3 signal only the trunk is depicted. Trace a (183 K, $R_0 = 2.17$ kHz, 4 s repetition delay): TOSS spectrum; the residual intensity of ssb + 1 of signal 4 results from incomplete suppression. Trace b (301 K, $R_0 = 3.66$ kHz, 10 s repetition delay): normal spectrum without ssb suppression. Trace c (parameters as before): NQS spectrum without ssb suppression; dephasing delay was 70 μs. The allyl signals have been completely suppressed, indicating immobility of the ligand.

In the ambient-temperature ^{13}C CP-MAS NMR spectra of **1a**,**b** the allyl meso carbon resonates at δ(C2) 93.8. For the triflate **1a** (Figure 7) the allyl methylene carbon signals are coalesced at ambient temperature, but they are separate at 183 K. The intensity of the OTf signal is low at 301 K, also when the repetition delay is long (100 s), which is explained by the mobility of this anion. For **1b-II** the methylene carbons afford two lines at δ(C1) 61.1 and δ(C3) 57.2, corresponding to an asymmetric allyl ligand, and these lines are little shifted at lower temperature (234 K). Additional ^{13}C CP-MAS NQS experiments[31] for **1a**,**b** at 301 K resulted in suppression of the allyl resonances, which is evidence for immobile allyl ligands on the time scale of this experiment. For **1b-II** the presence of an asymmetric allyl ligand and its firm coordination at ambient temperature are in obvious agreement with each other. The fact that the likewise immobile allyl ligand in **1a** has evidently symmetrical surroundings on the time average at ambient temperature may result from the mobility of the OTf anion. Complexes **1a**,**b** show only one ^{13}C singlet for the three PMe_3 ligands. This singlet is unchanged in the NQS spectrum due to rotations of the methyl groups and the individual ligands.

The limiting solid-state NMR spectra of **1a**,**b** are consistent with C_1-symmetrical ground-state structures of the cations. As has been confirmed by the molecular structure determinations, *TBP*-5 geometry is assumed for **1a**,**b**, in which the allyl ligand occupies an axial and an equatorial site, leaving two equatorial sites and an axial site for the three PMe_3 ligands. Thus, the two high-field resonances displaying the large J(PP) coupling of 130 Hz are attributed to P2 and P3 of the equatorial PMe_3 ligands, for which the P−Ni−P angle is widest (∼110°).[32] While P2 is located exo to allyl, P3 is endo and its coordination should be weakest; therefore, its high-field resonance comes closest to that of uncoordinated PMe_3 (δ(P) −61.4). This assignment is also suggested by the results of a density functional theoretical (DFT) study (see below). The low-field resonance δ(P1) is thus attributed to the most strongly bound axial PMe_3 ligand. This ligand lies at angles of ∼100° to the two equatorial PMe_3 ligands. Although these angles are only slightly smaller than the angle between the two equatorial PMe_3 ligands, the corresponding J(PP) couplings are significantly smaller, indicating that J(PP) couplings are a very sensitive probe for the size of the P−Ni−P angles.

[(η^3-C_3H_5)Ni(PMe_3)$_3$]Y (Y = Br (1c), I (1d)). According to the DSC spectra and X-ray powder diffractometry the microcrystalline PMe_3 halide complexes **1c**,**d** are polymorphic and undergo reversible endothermic transitions between two closely related phases, similar to the case for **1b**. The transitions are observed (DSC) for the bromide **1c** at −18 °C (255 K) (Figure S2) and for the iodide **1d** at −55.5 °C (218 K) (Figure S3) and thus are at relatively low temperatures, while the melting points are in the range of 140 °C. The enthalpies and entropies of the transitions between phases II and I are rather small compared to the corresponding enthalpies and entropies of fusion, as is already evident from a qualitative inspection of Figures S2 and S3. The small magnitude of the values excludes that a major property change is associated with these solid−solid phase transitions, which presumably also represent λ transitions.

X-ray powder diffraction studies confirmed that **1c**,**d** undergo reversible transitions between two crystalline phases in the temperature ranges manifested by the DSC measurements. The X-ray powder diffraction pattern of **1c-II** at 238 K, sufficiently below the phase transformation temperature of 255 K determined by DSC, is shown in Figure S4, trace a. Indexing of the diffraction pattern led to monoclinic symmetry. Although we could not identify the space group unambiguously, the space groups $P2_1/n$ and Pn were among the most likely candidates. After transition into phase **I**, the space group of the sample measured at 263 K (trace b) was determined to be $P4_2$ or $P4_1$ with $a = 8.781$ Å and $c = 12.418$ Å. Phase **I** is stable up to at least 323 K, as is evidenced by the concurrent diffraction pattern (traces b and c).

For **1d** (DSC transition at 217.5 K) the powder diffraction pattern of phase **II** was measured at 208 K and was likewise indexed for monoclinic symmetry (Figure S5, trace a). The space group could be reduced to a primitive cell with either the space group $P2_1/n$ or Pn. Increase of the temperature to 228 K (trace b) led to the formation of phase **I** with tetragonal symmetry and the most likely space group $P4_2$, and the lattice parameters $a = 8.925$ and $c = 12.619$ Å. Further increasing the temperature to 273 and 323 K (traces c and d) merely resulted in an increase of the unit cell parameters. Subsequent cooling of the sample back to 208 K led to resumption of the monoclinic LT phase (trace e).

The ambient-temperature solid-state NMR spectra of **1c**,**d** correspond to the HT phases of the complexes. The ^{31}P resonance of the bromide **1c-I** at 301 K is an apparent singlet ($w_{1/2} = 65$ Hz) with sidebands, typical for solid-state NMR (Figures S6 and S7). Some structuring of the signal, best visible for the sidebands, indicates either that coalescence of the ^{31}P

(31) The NQS (nonquaternary suppression) experiment takes advantage of the fact that the ^{13}C signals of CH and CH_2 *in motion* (as for quaternary carbons and rotating CH_3) do not vanish during a dephasing delay, since dipolar interactions to protons in the surrounding area are ineffective. (a) Opella, S. J.; Frey, M. H. *J. Am. Chem. Soc.* **1979**, *101*, 5854. (b) Alemany, L. B.; Grant, D. M.; Alger, T. D.; Pugmire, R. J. *J. Am. Chem. Soc.* **1983**, *105*, 6697.

(32) Wu, G.; Wasylishen, R. E.; Curtis, R. D. *Can. J. Chem.* **1992**, *70*, 863.

resonances is not yet complete or that an ABC spin system with very close chemical shifts is present. Thus, the dynamics of the PMe_3 ligands in **1c-I**, if occurring at all, are rather slow. A very similar spectrum is observed for the iodide **1d-I** between 254 and 221 K (Figure 8, traces b and c).

When the solids are gradually heated, that is, **1c-I** from 301 to 370 K (Figure S7) and **1d-I** from 254 to 314 K (Figures 8 and S9), the pseudo-singlets broaden substantially ($w_{1/2} \geq 800$ Hz), before at still higher temperature the line width diminishes again, as was found for **1d** (Figure S9). A similar line behavior has been previously observed in the VT ^{13}C CP-MAS NMR spectra of highly symmetrical organic molecules,[33a] of certain elastomers above the glass-transition temperature,[33b] and also of a metal complex.[33c] There, the change in line width as a function of the temperature (for a constant rotational frequency) is explained by a modulation of the CH dipolar coupling because of motions of the molecules or molecular fragments; that is, the suppression of the CH dipolar coupling by cross-polarization becomes inefficient when the frequency of motion approaches that of the decoupling field.[33b] Such an explanation also apparently holds for the observed ^{31}P line broadening in the present study. (No substantial change of the line width of the PMe_3 methyl signal of **1d** is found in the VT ^{13}C CP-MAS spectra.)

The ambient-temperature ^{13}C CP-MAS NMR spectra of **1c-I** and **1d-I** furnish three signals for the allyl ligands, which are thus asymmetric. It has been shown for **1d-I** that these lines are preserved when the sample is heated to 361 K (as they are also essentially unchanged at low temperature). Interestingly, in the ^{13}C CP-MAS NQS experiment at ambient temperature there is no suppression of the allyl resonances of **1c-I** and **1d-I**, evidence that *mobile* allyl ligands on the time scale of this experiment are present. The apparent discrepancy between an asymmetrically coordinated, but at the same time mobile, allyl ligand is resolved by the fact that the NQS experiment runs on a slower time scale than line-shape analysis (thus, slow dynamic processes already detected by the NQS experiment are not yet reflected in the line shape).

When for **1c-I** the temperature is lowered slightly below 256 K (Figure S8) and for **1d-I** slightly below 220 K (Figure S10), the complexes transform from phases **I** into the LT phases **II**. The ^{31}P pseudo-singlet vanishes, and three new resonances arise, corresponding to three inequivalent PMe_3 ligands. The new resonances are resolved for **1c-II** at 250 K and for **1d-II** at 216 K. Further lowering of the temperature only slightly improves the resolution. Nevertheless, the limiting ^{31}P spectrum of the bromide **1c-II** is observed at 183 K and that of the iodide **1d-II** at as low as 167 K. The changes in the spectra are reversible. The structures of **1c-II** and **1d-II** are almost rigid, while somewhat faster dynamics of the phosphorus ligands and the allyl group occur for **1c-I** and **1d-I**. It seems that the rate k of the structural dynamics is faster for the iodide **1d** than for the bromide **1c** in both phases **II** and **I** (eq 2b).

$$k_{1c}(\mathrm{Br}) < k_{1d}(\mathrm{I}) \qquad (2b)$$

In their limiting low-temperature ^{31}P CP-MAS spectra the halides **1c-II** and **1d-II** differ from **1a** and **1b-II** with respect to the chemical shift of P2 and the couplings. For the iodide **1d-II** (Figure 8; cf. Figure 19) the resonance of P2 is shifted to low field and there are now two close low-field doublets at

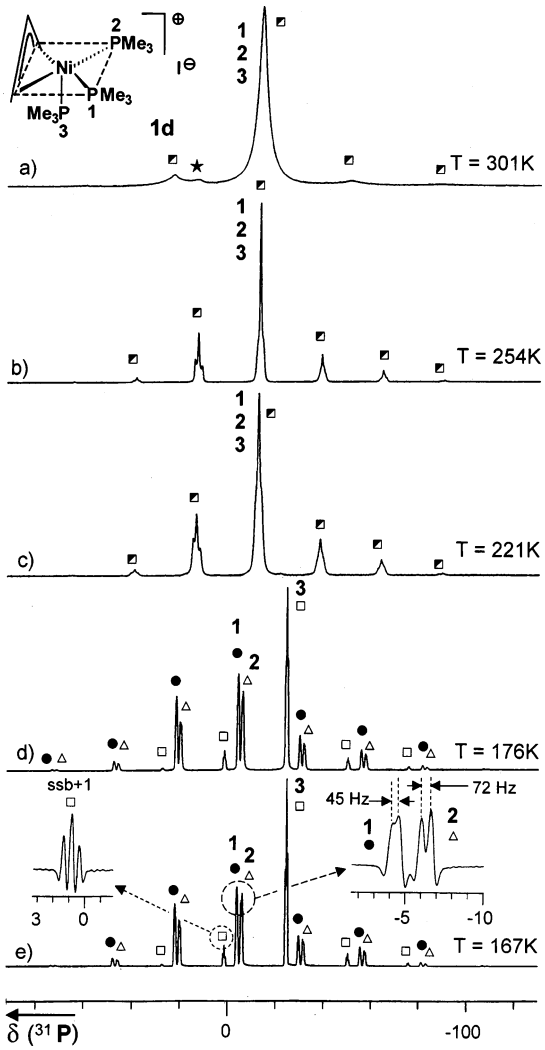

Figure 8. VT ^{31}P CP-MAS NMR spectra of **1d** at 167−301 K (see also Figures S9 and S10). Traces a−c describe **1d-I** and traces d and e **1d-II**. Trace a (301 K, $R_0 = 4.44$ kHz, 10 s repetition delay): a broad, unresolved signal ($w_{1/2} = 510$ Hz) is flanked by small first-order spinning sidebands (ssb + 1 and ssb − 1). The line width depends on the rotational frequency ($R_0 = 2.2$ kHz, $w_{1/2} = 1400$ Hz; $R_0 = 5.2$ kHz, $w_{1/2} = 500$ Hz). The asterisk marks an impurity. Trace b (254 K, $R_0 = 3.13$ kHz, 6 s repetition delay): the spectrum corresponds to that of **1c-I** at 301 K (see Figure S6, trace a). A pseudo-singlet is flanked by sidebands up to the third order (ssb ± 3). Trace c (221 K, $R_0 = 3.13$ kHz, 4 s repetition delay): the main line has become somewhat broader at its basis but is otherwise unchanged compared to trace b. Trace d (176 K, $R_0 = 3.13$ kHz, 4 s repetition delay): there are three signals with distinctly different anisotropic patterns, and the numbers mark their isotropic chemical shifts. The two low-field signals at δ(P1) −4.7 (●) and δ(P2) −6.6 (△) have very similar chemical shifts, line widths, and ssb patterns. In contrast, δ(P3) −24.8 (□) lies at makedly higher field and shows some fine structure and rather small sidebands of equal intensity. The intensity of the second-order sidebands, ssb ± 2, is almost zero. Trace e (167 K, $R_0 = 3.13$ kHz, 4 s repetition delay): the chemical shifts of the resonances are almost constant (δ −4.5, −6.7, and −24.9). The splitting of P3 has further increased. The inset on the right shows the region of the isotropic chemical shifts of signals 1 and 2 and the inset on the left ssb + 1 of signal 3. (The spectra of traces b−e have been subjected to Gaussian multiplication prior to FT for an improved resolution.) See also Table 5.

δ(P1) −4.4 and δ(P2) −6.4 and one high-field pseudo-triplet (unresolved doublet of doublets) at δ(P3) −24.9. The coupling

(33) (a) Rothwell, W. P.; Waugh, J. S. *J. Chem. Phys.* **1981**, *74*, 2721. (b) Voelkel, R. *Angew. Chem.* **1988**, *100*, 1525; *Angew. Chem., Int. Ed. Engl.* **1988**, *27*, 1468. (c) Vierkötter, S. A.; Barnes, C. E.; Garner, G. L.; Butler, L. G. *J. Am. Chem. Soc.* **1994**, *116*, 7445.

J(P2P3) has diminished to 72 Hz, and *J*(P1P3) has increased to 45 Hz, while *J*(P1P2) is small (<30 Hz) and is not resolved. The sideband pattern of the resonances is likewise informative. Thus, the anisotropic regions of P1 and P2 both extend over 180 ppm, whereas the anisotropic region of P3 is limited to about 100 ppm and its sideband pattern is typical for symmetrical surroundings of the ^{31}P nucleus (the intensities of ssb ± 1 are about the same and amount only to a few percent of the total intensity of the P3 signal).[34] For the bromide **1c-II** (Figure S6) δ(P2) −10.1 is about halfway between δ(P1) and δ(P3), and the resonances of P2 and P3 appear as doublets with *J*(P2P3) = 100 Hz, which is intermediate between the values found for **1a**,**b** and **1d**. The smaller couplings are not resolved. The anisotropic regions of P1 and P2 reach 130 ppm, and the ssb pattern for P3 is similar to that in **1d-II**. The calculated mean of the chemical shifts of the individual ^{31}P resonances of **1c-II** and **1d-II** agrees well with the shift of the coalesced resonances and with that in solution.

The limiting solid-state ^{13}C and ^{31}P NMR spectra of **1c-II** and **1d-II** are consistent with C_1-symmetrical ground-state structures of the cations. In contrast to the *TBP*-5 structure of **1a**,**b**, the LT ^{31}P CP-MAS NMR spectrum of the iodide **1d-II** is explained by a *SPY*-5 structure with P1 and P2 being tightly bound at the basal sites in a rather similar coordination mode, in agreement with two close low-field resonances, whereas P3, which resonates at markedly higher field, is more weakly coordinated at the endo apical site. While the coupling *J*(P1P2) between the basal ligands is small and is not resolved (<30 Hz), the observed couplings between these ligands and the apical PMe_3 ligand are of the usual magnitude (45 and 72 Hz). For the bromide **1c-II** the ground-state geometry of the cation seems related to the *SPY*-5 structure of **1d-II**, but perhaps somewhat more distorted with respect to *TBP*-5, as evidenced by the chemical shifts of the ^{31}P resonances, their couplings, and the ssb patterns.

[(η^3-C_3H_5)Ni{$P(OMe)_3$}$_3$]OTf (2a). When the crystallized $P(OMe)_3$ triflate **2a** is heated in the DSC from −40 °C at a rate between 5 and 1 K min^{-1}, the somewhat broad endothermic solid-phase−solid-phase transition **2a-II** → **2a-I** is found at −21 °C (252 K), while the complex decomposes exothermically without melting only above 130 °C. The reverse of the endothermic effect is observed at −34 °C. It splits at low cooling rates into numerous events. Thus, at a cooling rate of 0.5 K min^{-1} a statistical distribution of small but sharp exothermic effects is found, which can be attributed to the presence of individual crystallites with different nucleation energies (Figure 9). There is some dependency of the transition temperatures and the shape of the curve on the individual sample, but the main features of the spectrum remain unchanged. Integration of a spectrum at heating and cooling rates of 5 K min^{-1} gave for **2a-II** → **2a-I** an enthalpy of transition of $\Delta H_{252\ K}$ = 12.5 kJ mol^{-1} and an entropy of transition of $\Delta S_{252\ K}$ = 49.6 J K^{-1} mol^{-1}. The magnitude of these values and also the supercooling in the range of 10−15 K are quite in contrast to the properties of **1b**−**d**.

Further experiments suggest that **2a-II** is crystalline and **2a-I** a plastically crystalline phase. No single-crystal X-ray structure analysis has been possible for **2a** in either phase. However, the powder diffraction pattern of **2a-II** measured at 228 K revealed crystallinity, and it was indexed for triclinic symmetry (Figure 10, trace a). In contrast, the powder pattern of **2a-I** collected at 268 K exhibits a reduced number of reflections (7) in the range from 7 to 31° in 2θ (trace b). These peaks can be assigned to a CsCl-type cubic lattice with a = 8.862 Å.

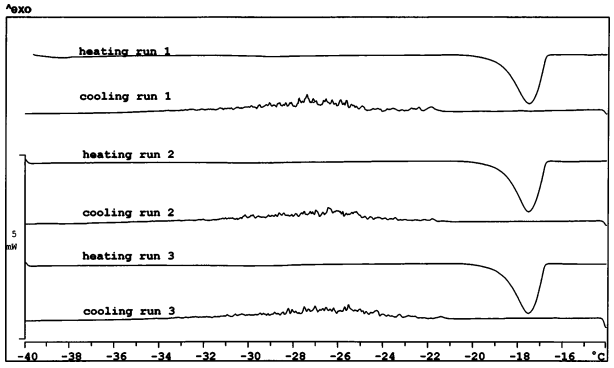

Figure 9. DSC spectrum of [(η^3-C_3H_5)Ni{$P(OMe)_3$}$_3$]OTf (**2a**) between −40 and −14 °C at a heating and cooling rate of 0.5 K min^{-1}. For the given sample the endothermic effect is observed at −17 °C and the exothermic reverse between −32 and −22 °C (centered at −27 °C) as a statistical distribution of numerous small effects.

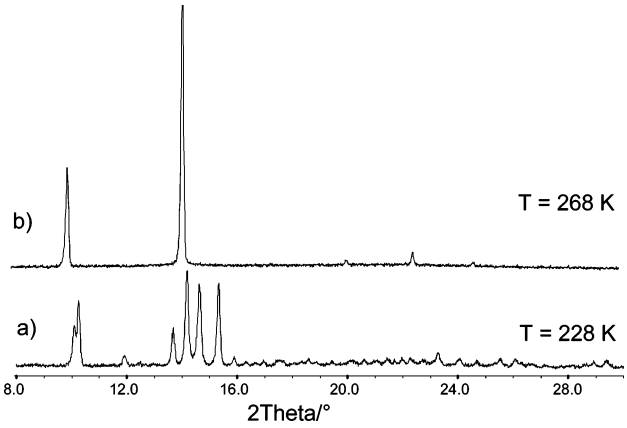

Figure 10. X-ray powder patterns for **2a**. Trace a: triclinic **2a-II** at 228 K. Trace b: plastically crystalline **2a-I** at 268 K with a cubic primitive cell (DSC transition temperature 253 K).

In the ambient-temperature ^{31}P CP-MAS NMR spectrum of **2a-I** (Figure S11, trace a) the three $P(OMe)_3$ ligands give rise to a very narrow line at δ(P) 138.8 ($w_{1/2}$ = 10 Hz), which is flanked by small first-order spinning sidebands. The spectrum resembles a solution NMR spectrum. In the ^{13}C CP-MAS NMR spectrum (Figure S12, trace b), in addition to the OTf quartet, narrow single lines are observed for the central allyl carbon at C2, the equivalent terminal allyl methylene groups C1/C3, and the three equivalent $P(OMe)_3$ ligands. The NQS spectrum (trace c) is practically unchanged, indicating that the allyl ligand is mobile. The intensity of the OTf signal in the CP-MAS NMR spectrum is low, whereas it is as expected in the MAS NMR spectrum. Since cross-polarization seems less effective than direct excitation, we conclude that the OTf ligand is also mobile. Thus, the solid-state NMR spectra indicate that all ligands of the cation and the OTf anion are mobile for **2a** in phase I.

When **2a-I** is cooled to 237 K (−36 °C) to afford **2a-II**, the ^{31}P NMR line splits into various unresolved signals, which further change their appearance upon cooling to 176 K (Figure S11). In the ^{13}C NMR spectrum the resonances of the allyl terminal C atoms are broad at 194 K (and also 176 K), and for the OMe groups several unresolved resonances are observed (Figure S12). Obviously, the limiting ^{13}C and ^{31}P NMR spectra of **2a-II** have not yet been reached. It seems possible that the

(34) Symmetrical ssbs of low intensity that are confined to a relatively small anisotropic region have also been observed for the apical PMe_3 ligand in [(η^3-C_3H_5)Ni(dmpe)(PMe_3)]Y complexes, for which an *SPY*-5 structure has been proved by X-ray crystallography.[20b]

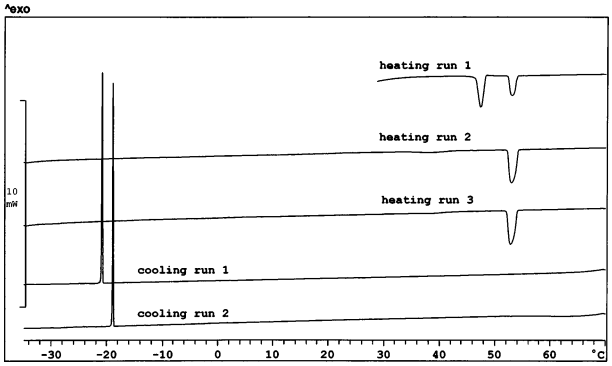

Figure 11. DSC spectrum of $[(\eta^3\text{-}C_3H_5)Ni\{P(OMe)_3\}_3]PF_6$ (**2b**). Heating and cooling rates: 1 K min^{-1}. After crystallization **2b-III** was kept cold until recording of the spectrum, when it was briefly warmed to ambient temperature and DSC was started (it has been checked that there is no signal below this temperature). Heating the pristine **2b-III** caused a first endothermic transition at 47 °C (irreversible in the DSC) into phases **2b-II** and **2b-I** to an about equal extent. The second endothermic effect at 53 °C is due to the transformation of the partly formed **2b-II** into **2b-I** (heating run 1). When the sample is cooled again, the compound resumes phase II at −21 °C (cooling run 1). During the second and further cycles reversible transformations occur between phases **II** and **I**.

changes in the spectra result from the formation of a mixture of isomers, which may arise from different conformations of the $P(OMe)_3$ ligands, in agreeement with the DSC of **2a** and a DFT study on **2** (see below). A determination of the ground-state structure of **2a** (*TBP*-5 vs *SPY*-5) has not been possible by X-ray structure analysis or on the basis of the NMR spectra. Nevertheless, because of similar anisotropic regions and ssb patterns of **2a-II** and the established *TBP*-5 complexes we presume **2a-II** to have a formal *TBP*-5 structure (as for the PF_6 salt **2b** and the iodide **2d**, but in contrast to the bromide **2c**).

In summary, complex **2a** forms the two phases **II** and **I**. The LT phase **I** is shown to be crystalline, but a determination of the ground-state structure of the complex was not possible. At 252 K phase **II** transforms into phase **I**. The various properties of this solid phase, in particular the high entropy of transition, the marked supercooling, a primitive cubic cell, and solution-type solid-state ^{13}C and ^{31}P NMR spectra, all indicate a high degree of disorder and mobile cations and anions with isotropic surroundings; thus, that we conclude that phase **I** represents an orientationally disordered or plastically crystalline mesophase.

$[(\eta^3\text{-}C_3H_5)Ni\{P(OMe)_3\}_3]PF_6$ (2b). More detailed information about the phase transitions of the PF_6 salt **2b** (eq 1) was obtained from DSC measurements (Figure 11). When pristine **2b-III**, as it was crystallized at 0 °C or below and kept cool, is heated in the DSC at a rate of 1 K min^{-1}, it undergoes an endothermic transition at 47 °C, presumably into a mixture of the high-temperature crystalline phase **2b-II** and the plastically crystalline phase **2b-I**. Under DSC conditions with relatively rapid heating the transformation **2b-III** → **2b-II** occurs at a higher temperature than the ambient temperature at which, according to eq 1, the transition proceeds only slowly.

There is a further endothermic transition at 53 °C when **2b-II** transforms fully into the plastically crystalline **2b-I**. Cooling results in an exothermic effect only at −20 °C. Subsequent repeated heating and cooling cycles merely show the endothermic transition at 53 °C and a sharp but somewhat fluctuating exothermic transition at about −20 °C, which corresponds to a supercooling of >70 K (Figure 11). The magnitude of the supercooling remains unchanged when a delay of several hours is included in the cooling run. The supercooling is only observed when **2b-I** is heated well above the formation temperature of 53 °C, suggesting that some ordering of the system remains above the transition temperature. If the endothermic signal is truncated, the exothermic reverse transition occurs as high as 40 °C, consistent with residual domains of the previous **2b-II**. The single sharp DSC signal for the **2b-I** → **2b-II** transition is quite in contrast to the numerous small signals observed for the **2a-I** → **2a-II** transformation (Figure 9). Clearly, nucleation of the **2b-II** phase inside the **2b-I** phase is difficult (hence the large supercooling), but it would appear that once a nucleus has been formed the phase transformation goes to completion almost instantaneously for the whole sample.

In a separate experiment pristine **2b-III** was heated in a flask at 55 °C for 30 min and then quenched by immersing the flask in liquid nitrogen. The subsequently recorded DSC heating run (started at −60 °C) showed the transformation **2b-II** → **2b-I** at 53 °C and gave no indication of the presence of **2b-III**. Thus, quenching **2b-I** gave **2b-II** but no **2b-III**. The result is in agreement with the Ostwald−Volmer rule,[35] according to which the less dense phase is formed first when a polymorphic system is cooled. At low temperature (<0 °C) **2b-II** is metastable with respect to **2b-III**, but the rate of conversion is very low (eq 1). The DSC curve of **2b** is basically unchanged for higher heating and cooling rates (up to 10 K min^{-1}), although at this rate the transitions at 47 and 53 °C merge. The enthalpy and entropy of transition were determined for **2b-II** → **2b-I** to be $\Delta H_{326\ K}$ = 19.3 kJ mol^{-1} and $\Delta S_{326\ K}$ = 59.2 J K^{-1} mol^{-1}, indicating the appearance of significant structural disorder. From the difference between these values and those for the combined **2b-III** → **2b-II** → **2b-I** transitions of about $\Delta H \approx 24$ kJ mol^{-1} and $\Delta S \approx 74$ J K^{-1} mol^{-1} the enthalpy and entropy for the crystalline−crystalline transition **2b-III** → **2b-II** was estimated at $\Delta H_{320\ K} \approx 4.7$ kJ mol^{-1} and $\Delta S_{320\ K} \approx 15$ J K^{-1} mol^{-1}, in agreement with a minor, but nevertheless marked, structural reorientation of the molecules. The combined melting and subsequent decomposition at about 130 °C represent also merely a minor thermic effect.

In an X-ray powder diffraction study a sample of **2b-III** was ground at −78 °C, mounted in the cold stream on the diffractometer, and maintained at 100 K. The observed powder diffraction data (Figure 12, trace a) are in good agreement with the pattern calculated from the crystallographic data of the single-crystal study. When **2b-III** is warmed to 288 K, the analysis of the powder pattern merely shows the expansion of the unit cell due to the thermal motion of the atoms (trace b). However, an increase of the temperature to 333 K results in a drastic simplification of the diffraction pattern (trace c), similar to that observed for **2a-I**. The new pattern can be indexed for a CsCl-type cubic primitive cell with a latice parameter of 8.811 Å, and we attribute it to the formation of the plastically crystalline phase **2b-I**. The cell volume V = 684 $Å^3$ is markedly larger than the molecular volume of **2b-III** at ambient temperature (645 $Å^3$). Lowering the temperature to 288 K gives rise to a new powder diffraction pattern which cannot be indexed unambiguously but which can be assigned to crystalline **2b-II** (trace d). Further cooling to 100 K leads to a contraction of the unit cell of **2b-II** (trace e), instead of re-formation of the starting phase **2b-III**. Heating **2b-II** to 333 K results in re-formation of **2b-I** (trace f).

Concomitant with the DSC and X-ray studies on **2b** a detailed solid-state NMR investigation was carried out. We first describe

(35) (a) Volmer, M. In *Die Chemische Reaktion*; Bonhoeffer, K. F., Ed.; Steinkopff: Dresden, Germany, 1939; Vol. IV (Kinetik der Phasenbildung). (b) Holleman, A. F.; Wiberg, E. *Lehrbuch der Anorganischen Chemie*, 101st ed.; de Gruyter: Berlin, 1995; p 543.

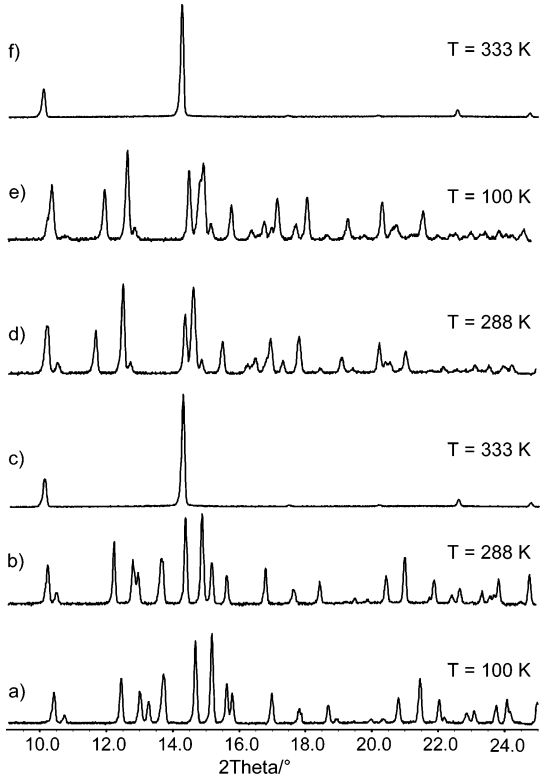

Figure 12. X-ray powder diffraction patterns of **2b** in various phases. Traces a and b: monoclinic **2b-III** at 100 and 288 K. Trace c: plastically crystalline **2b-I** at 333 K, just above the DSC phase transition temperature of 326 K. The spectrum corresponds to a cubic primitive cell. Traces d and e: crystalline **2b-II**, obtained from **2b-I**, at 288 and 100 K. Trace e: reconversion of **2b-II** into **2b-I** at 333 K.

the spectra of pristine **2b-III**, which was kept cold until recording of the spectra at 301 K. In contrast to all the aforementioned complexes **1a**−**d** and **2a**, the structure of the cation of **2b-III** is rigid in the solid state at ambient temperature. In the ^{31}P CP-MAS NMR spectrum (Figures 13 and 14, each with trace a) three sharp resonances with fine structures were observed for P1, P2, and P3 spread over a range of 21.6 ppm. The calculated mean of the chemical shifts (δ(P) 139.9) corresponds closely to the chemical shift observed for the complex in solution (δ(P) 140.2). As for the PMe_3 complexes, the low-field resonance of P1 is an apparent singlet, and a pair of doublets of doublets is found for P2 and P3. The coupling of the latter at J(P2P3) = 211 Hz is surprisingly large,[30] while the couplings between P1 and P2 or P3 are much smaller (cf. Figure 19). The spectrum is unchanged at 233 K. The spectral data are best explained by a *TPB*-5 structure of **2b-III**, and this has been confirmed by X-ray analysis (see above). The magnitudes of the chemical shifts of the individual phosphorus atoms appear to correlate inversely with the lengths of the respective Ni−P bonds (2.15, 2.18, and 2.21 Å); that is, the shorter (stronger) the Ni−P bond, the greater the deshielding of the nucleus. The assignment of P1 to the axial, P2 to the exo equatorial, and P3 to the endo equatorial phosphite ligand has been qualitatively confirmed by a DFT calculation of the resonances. In the ambient-temperature ^{13}C CP-MAS spectrum of **2b-III** (Figure S13, trace a) three resonances reveal an asymmetric allyl ligand. The NQS experiment results in suppression of these resonances, confirming the static nature of the ligand.

When a sample of **2b-III** is left at ambient temperature for some time, the solid-state NMR spectra change gradually (Figure

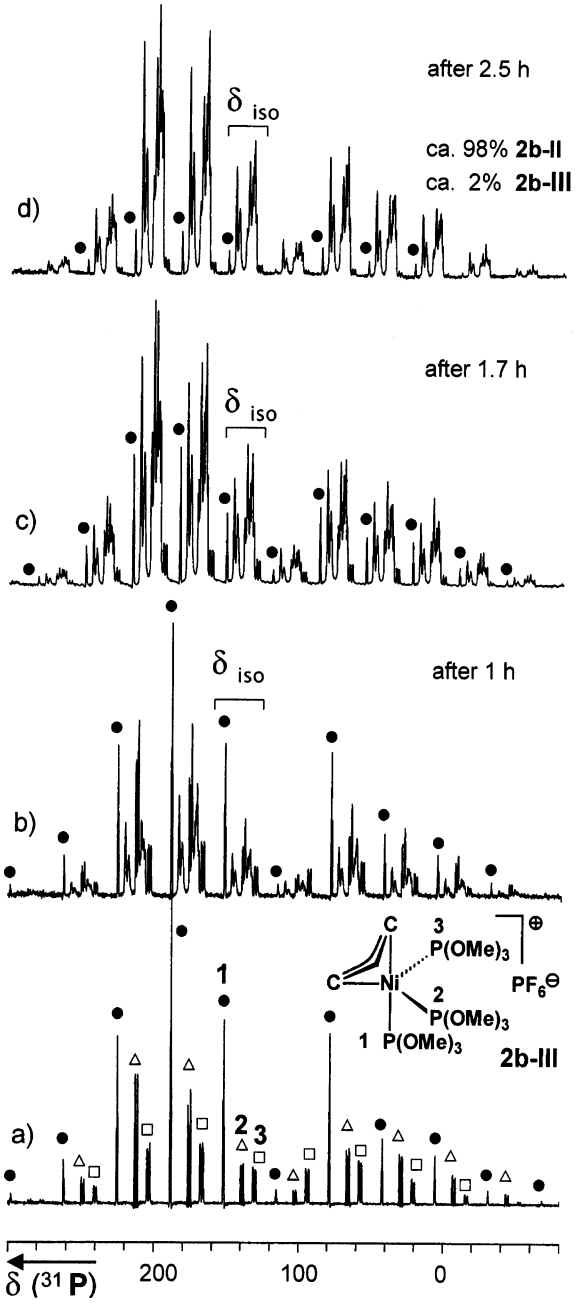

Figure 13. ^{31}P CP-MAS NMR spectra of **2b-III** at 301 K (PF_6 signal omitted). Trace a (R_0 = 4.44 kHz, 20 s repetition delay): the spectrum of the freshly synthesized **2b** shows three well-resolved signals. The numbers mark the isotropic chemical shifts: (●) signal of P1 and corresponding ssb; (△) signal of P2 and ssb; (□) signal of P3 and ssb. Trace b (R_0 = 4.44 kHz, 30 s repetition delay): the spectrum has been recorded after the probe has been kept in the rotor at 22 °C for 1 h. The spectrum contains in addition to the signals of **2b-III** (only the signals of P1 (●) have been labeled for clarity) two new groups of partially well-resolved signals, attributed to **2b-II**. Trace c (R_0 = 3.91 kHz, 20 s repetition delay): spectrum of the same probe after 1.7 h at 22 °C. The transformation **2b-III** → **2b-II** has further progressed, and the intensity of the signals of the starting phase **2b-III** is markedly reduced. Trace d (R_0 = 3.91 kHz, 10 s repetition delay): spectrum of the same probe after a total of 2.5 h at 22 °C. The spectrum shows essentially the signals of **2b-II**, but traces of the starting phase **2b-III** are still visible. For the particular sample the half-time for the transformation **2b-III** → **2b-II** at 22 °C is estimated to be 30 min. All spectra have been subjected to Gaussian multiplication prior to Fourier transformation to improve resolution.

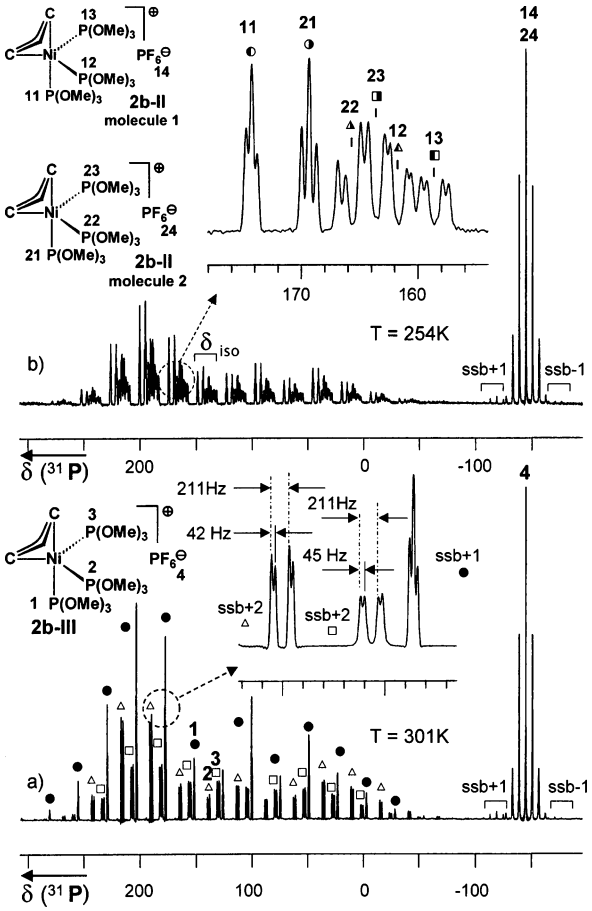

Figure 14. Comparison of the ^{31}P CP-MAS NMR spectra of the two crystalline phases **2b-III** and **2b-II**. Trace a (301 K, $R_0 = 3.13$ kHz, 20 s repetition delay): spectrum of the freshly synthesized **2b-III**. The numbers 1 (●), 2 (△), and 3 (□) mark the isotropic chemical shifts and the symbols the corresponding sidebands. The inset shows an enlargement of ssb + 2 for P2 and P3 and of ssb + 1 for P1. Trace (b) (254 K, $R_0 = 4.44$ kHz, 6 s repetition delay): Spectrum of the rearrangement product **2b-II**, containing two inequivalent molecules in the elementary cell. The phosphorus atoms 11 (◐), 12 (▲), 13 (◧) and 21 (◑), 22 (▲), and 23 (◨) have been assigned to the two molecules on the basis of their J(PP) coupling constants. These have been confirmed by the 2D J-resolved ^{31}P CP-MAS spectrum at this temperature. The inset shows an enlargement of ssb + 1. δ_{iso} marks the region of the isotropic chemical shift. Both spectra have been subjected to Gaussian multiplication prior to Fourier transformation. For further details, see Table 5.

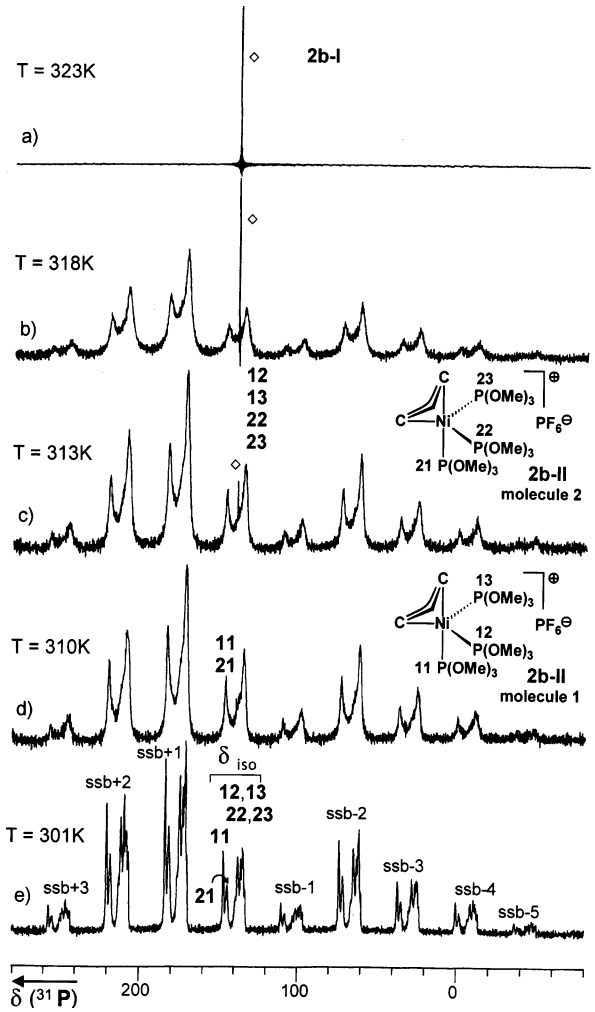

Figure 15. VT ^{31}P CP-MAS NMR spectra of **2b-II** and **2b-I** at 301−323 K (PF_6 signal omitted; see also Figures 13, 14, and S13). The spectra of all traces ($R_0 = 4.44$ kHz, 10 s repetition delay) have been recorded after temperature adjustment periods of 1 h. Trace a (323 K): the spectrum ($w_{1/2} = 25$ Hz) resembles that of a solution and is attributed to the plastic crystal phase (◇) **2b-I**. Trace b (318 K): besides the sharp singlet for minor amounts of **2b-I**, a signal pattern has appeared that is typical for an anisotropic solid state, in which the signals are broadened due to a dynamic structure. It is assigned to the ordered crystal of **2b-II**. Trace c (313 K): only a trace of the plastic phase is still visible, and the signals of **2b-II** have become sharper. Trace d (310 K): the lack of fine structure indicates a dynamic process involving the phosphorus ligands in the ordered crystal. Trace e (301 K): the emerging fine structure indicates that the dynamic process of the phosphorus ligands in **2b-II** has markedly slowed. This is best visible from signals 11 and 21, which are still coalesced at 310 K. The range of the isotropic chemical shift is marked δ_{iso}. The assignment of the lines, in particular for the phosphorus atoms 12, 13, 22, and 23 was made at an even lower temperature (see Figure 14, trace b, and Table 5). The spectra have been subjected to Gaussian multiplication prior to Fourier transformation.

13, traces a−d). The resonances of **2b-III** all vanish, and instead the spectrum of the new phase **2b-II** is observed. For well crystallized **2b-III** the transformation **2b-III** → **2b-II** takes only a few hours, but it may take even several days for crystals of lower quality. The complete conversion of **2b-III** to **2b-II** also occurs after heating the rotor to 36 °C for 107 min or briefly to 50 °C. The ^{31}P CP-MAS spectrum of **2b-II** is only partially resolved at ambient temperature (Figure 13, trace d, and Figure 15, trace e) but sharpens considerably upon cooling the probe to 254 K (Figure 14, trace b), indicating that slow dynamics are prevalent in **2b-II** (in contrast to **2b-III**). **2b-II** contains the two inequivalent molecules 1 and 2 in the exact ratio of 1:1. Both isomeric molecules of **2b-II** show the characteristics of a *TBP*-5 structure (as does **2b-III**); that is, in the ^{31}P NMR spectrum at low field an unresolved doublet of doublets with small couplings and at higher field a pair of doublets of doublets with a large coupling J(P2P3) > 200 Hz are observed (cf. Figure 19). Interestingly, although the mean of the chemical shifts of P1, P2, and P3 is about the same for all three isomers and corresponds to that in solution (δ(P) 139.5), the shift *range* of the resonances diminishes from 21.6 ppm (**2b-III**) to 12.7 and 7.8 ppm (**2b-II**, molecules 1 and 2). ^{13}C CP-MAS NMR of **2b-II** at 301 K (Figure S13, trace b) gave two sets of resonances for inequivalent and asymmetric allyl ligands and two types of $P(OMe)_3$ ligands, and suppression of the allyl resonances in the

NQS experiment showed that the allyl ligands are still static on the NMR time scale.

The solid-state NMR data of the complex **2b** in the crystalline phases **III** and **II** agree well with the data obtained by other physical methods. Thus, the NMR data on **2b-III** show that there is one type of ion pair present, consistent with the X-ray structure analysis, which reveals that the chiral unit cell contains two cations of identical chirality. The NMR data of this phase also show that the cation is rigid, which is consistent with the observation that this phase has the highest density (closest packing) according to DSC and assuming that the Ostwald−Volmer rule applies. When the temperature is raised above $T_c \approx 15$ °C (288 K), **2b-III** reversibly transforms into **2b-II** (eq 1). In the solid-state ^{13}C and ^{31}P NMR this transition **2b-III** → **2b-II** is marked by a doubling of the allyl and $P(OMe)_3$ ligand signals. In agreement with the larger cell volume of phase **2b-II**, VT solid-state NMR shows that the dynamics of the phosphorus atoms in **2b-II** are frozen out at a lower temperature than for **2b-III**, suggesting that the ions in the phase **2b-II** have more room for movement. Since the crystal **2b-III** is chiral, it is attractive to speculate that the doubling of the NMR signals during the transition **2b-III** → **2b-II** is a result of a diastereomeric effect caused by racemization of the cations in the chiral environment of the unit cell.[36]

Further changes in the ^{31}P CP-MAS spectrum are observed when **2b-II** is heated above ambient temperature (Figure 15). Between 301 and 313 K the signals broaden (traces c−e) and a small very sharp singlet (◇) at δ(P) 138.9 arises, which at 318 K represents perhaps 1% of the total intensity (trace b). This singlet can be attributed to the formation of the plastically crystalline phase **2b-I**. Since the phases **2b-II**/**-I** appear to coexist in this temperature range, we conclude that interstate equilibrium is slow. However, when the temperature is raised from 318 to 323 K, **2b-II** is completely converted into **2b-I** and only the ^{31}P NMR singlet at δ(P) 138.8 ($w_{1/2} = 25$ Hz) remains. The corresponding ^{13}C CP-MAS spectrum (Figure S13, trace c) displays two sharp resonances for a symmetrical allyl ligand, similar to a solution NMR spectrum. Since these resonances do not vanish in the NQS spectrum, the allyl group must be mobile, as are the phosphite ligands and possibly also the PF_6 anion. The change in the spectra corresponds to the phase transition detected by DSC at 53 °C (Figure 11). The spectral changes between **2b-II** and **2b-I** are fully reversible, and no supercooling is observed in the solid-state NMR spectra. This fact is explained either by residual domains of **2b-II** in the **2b-I** phase, serving as a seed crystal, or by rapid nucleation due to shear stress of the particles in the spinning rotor.

[(η^3-C_3H_5)Ni{$P(OMe)_3$}$_3$]Y (Y = Br (2c), I (2d)). Despite their different crystal structures, the DSC behavior of the $P(OMe)_3$ halide complexes **2c**,**d** is quite similar. The complexes show at a heating rate of 1 K min^{-1} a marked endothermic transition at about 50 °C (**2c**) or 68 °C (**2d**), which is immediately followed by an exothermic effect (for **2d**, see Figure 16). At these temperatures the crystalline complexes are seen to form viscous oils, which upon cooling solidify only slowly and partially to eventually give a semisolid material. Further effects occur only above 110 °C and result in decomposition. When samples of **2c**,**d** are heated just to the beginning of the endothermic transition and then cooled and reheated in a second run, both initial transitions are no longer observed. Thus, the endothermic and subsequent exothermic transitions

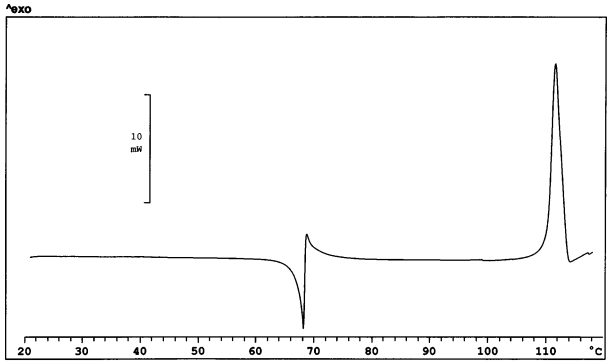

Figure 16. DSC spectrum of [(η^3-C_3H_5)Ni{$P(OMe)_3$}$_3$]I (**2d**) (heating rate 1 K min^{-1}).

seem closely related to each other. All effects are irreversible. By way of an explanation of the phase behavior, we assume that complexes **2c**,**d** crystallize from solution into a metastable phase. This phase melts at a relatively low temperature (endothermic transition), whereby the ions assume an energetically more favored orientation (superposed exothermic effect), although full crystallization of the new phase appears to be retarded. The nature of the new phases was not investigated further. Since X-ray single-crystal structure determinations of **2c**,**d** exist, no additional powder diffraction study was carried out.

The different molecular structures of **2c**,**d** are reflected in their solid-state NMR spectra. A characteristic feature of the ^{31}P CP-MAS NMR spectrum of the bromide **2c** at 301 K is a low-field pseudo-triplet (unresolved doublet of doublets) and two very close high-field doublets (Figure 17, trace a; see also Figure 19). The two close doublets can be attributed to P1 and P2 as basal ligands based on an *SPY*-5 structure for **2c**, as confirmed by X-ray structure analysis. Since these ligands are arranged at approximately right angles to one another, their coupling is small (<30 Hz) and is not resolved. The pseudo-triplet at δ(P) 149.9 can be attributed to the endo apical ligand P3. This ligand couples to the two basal ^{31}P nuclei, giving rise to the couplings J(P1P3) = 53 Hz and J(P2P3) = 61 Hz of medium magnitude. If one assumes that the coordination of P3 is relatively weak, the unexpected low-field position of the pseudo-triplet is consistent with the occurrence of the chemical shift of uncoordinated $P(OMe)_3$ (δ(P) 143.4) also at lower field than the resonances of P1 and P2. The mean of the three resonances (δ(P) 142.6) is about $\Delta\delta = 2-4$ ppm to lower field of the mean shifts of the solid *TBP*-5 complexes **2a**, **2b-III**/**-II**, and **2d**. (Since the solution NMR chemical shift of **2c**, δ(P) 139.7, corresponds to the mean shifts of the latter as a solid and in solution, it is probable that its structure in solution is also *TBP*-5.) According to the spectra the solid-state structure of **2c** is rigid at 301 K. The signal pattern resembles the limiting low-temperature spectrum of the dynamic PMe_3 complex **1d** (Figure 8, trace e), with the difference that the pseudo-triplet is at low field and not at high field from the doublets (cf. Figure 19).

In the ^{13}C NMR spectrum of **2c** (Figure 17, trace b) the allyl ligand gives rise to three resonances and hence is asymmetric and immobile. Its immobility is also revealed by suppression of the allyl resonances in the NQS spectrum. In the region of the OMe groups three signals at δ(C) 55.2, 52.9, and 49.2 with an intensity ratio of 7:1:1 are found. In view of the molecular structure of **2c**, the two small signals could possibly be due to the OMe substituents that are closest to the bromide.

Whereas the bromide **2c** adopts an *SPY*-5 structure in the solid, the iodide **2d** is *TBP*-5, as for **2b-III**/**-II**. The ^{31}P CP-

(36) For examples of a racemate crystallizing in a chiral space group, see: Brock, C. P.; Schweizer, W. B.; Dunitz, J. D. *J. Am. Chem. Soc.* **1991**, *113*, 9811.

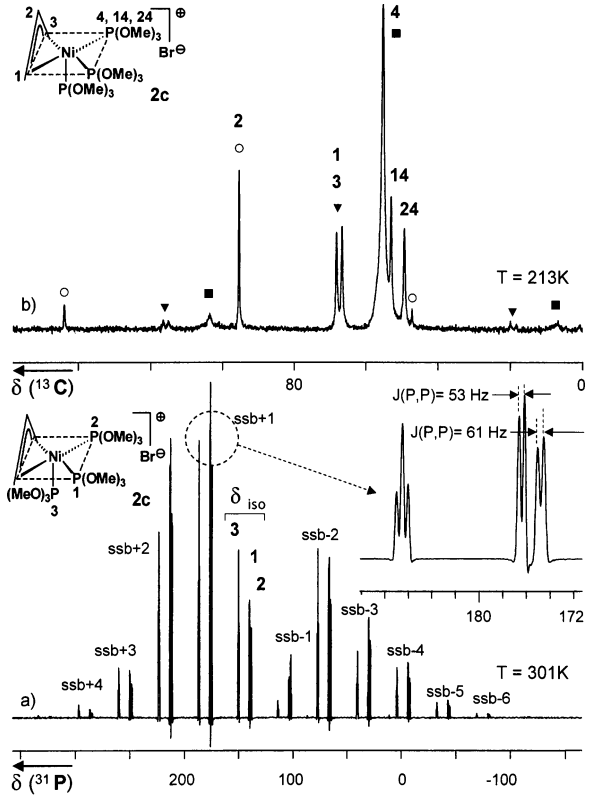

Figure 17. ^{13}C and ^{31}P CP-MAS NMR spectra of **2c**. Trace a, ^{31}P NMR (301 K, $R_0 = 4.44$ kHz, 20 s repetition delay): the signals of the three phosphorus atoms are well-resolved. The inset shows an enlargement of the splitting in the region of ssb + 1. The numbers mark the isotropic chemical shift. The splitting is independent of the rotational frequency. The values of the *J*(PP) couplings have been confirmed by 2D *J*-resolved ^{31}P CP-MAS NMR. The small coupling *J*(P2P3) ≤ 20−30 Hz could not be determined, due to some decomposition of the sample over the course of several hours at 301 K. Trace b, ^{13}C CP-MAS NMR (229 K, $R_0 = 3.65$ kHz, 10 s repetition delay): the asymmetric allyl group exhibits two signals for the terminal carbon atoms C1 and C3 (▼) and one for the central carbon C2 (○). The same symbols mark the corresponding sidebands. The C atoms of the $P(OMe)_3$ ligands give rise to three lines (4, 14, and 24) in the intensity ratio 7:1:1. The spectra have been subjected to Gaussian multiplication prior to Fourier transformation.

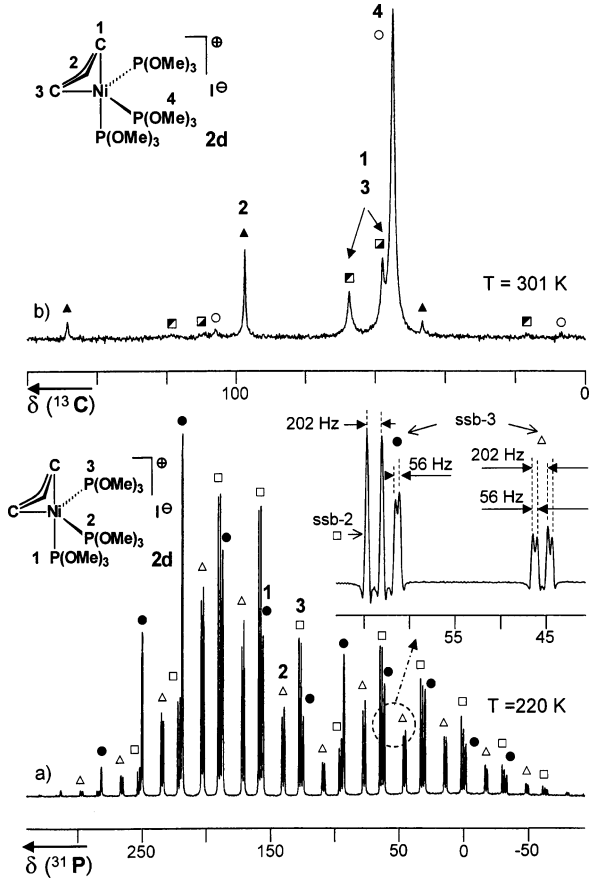

Figure 18. ^{13}C and ^{31}P CP-MAS NMR spectra of **2d**. Trace a, ^{31}P NMR (220 K, $R_0 = 3.82$ kHz, 12 s repetition delay): the signals of the three phosphorus atoms are well-resolved. The numbers mark the isotropic chemical shifts. The splitting is independent of the rotational frequency (cf. Figure S14, trace b). The inset shows an enlargement of the splitting in the region of ssb − 2 for signal 3 and ssb − 3 for signals 1 and 2 (after Gaussian multiplication). The small coupling *J*(P1P3) ≤ 20−30 Hz could not be determined. Trace b, ^{13}C CP-MAS NMR (301 K, $R_0 = 3.85$ kHz, 10 s repetition delay): the asymmetric allyl group exhibits two signals for the terminal carbon atoms C1 and C3 (◩, ◪) and one for the central carbon C2 (▲). The same symbols label the corresponding sidebands. The C atoms of the $P(OMe)_3$ ligands give rise to one line.

MAS NMR spectrum of **2d** at 220 K (Figure 18, trace a) displays a low-field doublet for the axial P1 and two partially resolved doublets of doublets for the equatorial P2 and P3. The equatorial coupling *J*(P2P3) = 202 Hz is again quite large, while the axial−equatorial coupling *J*(P1P2) = 56 Hz is of medium magnitude and *J*(P1P3) is not resolved. At ambient temperature the lines are somewhat broadened (Figure S14). The mean of the resonances (δ(P) 140.1) agrees exactly with the solution NMR chemical shift, suggesting the same structure in the solid state and in solution. The spectrum of **2d** essentially corresponds to that of **2b-III** (cf. data in Table 5), but the range of the chemical shifts is increased even further to 26.3 ppm and *J*(P1P3) has decreased.

The ambient-temperature ^{13}C CP-MAS NMR of **2d** shows a singlet for the $P(OMe)_3$ ligands and three resonances for an asymmetric allyl ligand (Figure 18, trace b). Suppression of the allyl resonances in the NQS spectrum is in agreement with immobility of this ligand in the crystal. All in all, the *TBP*-5 structure of solid **2d** appears to be less rigid than that of **2b-III** and the mobility of the $P(OMe)_3$ ligands resembles that of **2b-II**. The allyl ligands are consistently immobile for the two compounds in these phases.

DFT Calculations on 1 and 2. DFT calculations on the Ni cations **1** and **2** were performed in order to compare the experimentally determined structures with the calculated geometries and to model the structural dynamics of the complexes in solution and in the solid state. Although the calculations refer to the gas-phase structures of the complexes, there is generally good agreement between the calculated structures and the experimentally determined solid-state geometries. The angular parameters τ obtained for the experimental structures (X-ray), the calculated gas-phase structures, and the transition states for the dynamics are given in Table 6. For early theoretical considerations on the bonding of allyl ligands, see ref 37. For (η^3-C_3H_5)$Co(CO)_3$ a small rotational barrier of 2.9 kcal/mol has

(37) (a) Albright, T. A.; Hofmann, P.; Hoffmann, R. *J. Am. Chem. Soc.* **1977**, *99*, 7546. (b) Harlow, R. L.; McKinney, R. J.; Ittel, S. D. *J. Am. Chem. Soc.* **1979**, *101*, 7496. (c) Mingos, D. M. P. In *Comprehensive Organometallic Chemistry*; Wilkinson, G., Ed.; Pergamon: Oxford, England, 1982; Vol. 3, Chapter 19, pp 60−67. (d) Goddard, R.; Krüger, C.; Mark, F.; Stansfield, R.; Zhang, X. *Organometallics* **1985**, *3*, 285.

Table 6. Angular Parameter τ for Cationic $[(\eta^3\text{-allyl})NiL_3]^+$ Complexes[a]

	L	α^b	β^b	τ
1a	**PMe_3**	**156.3**	**135.0**	**0.35**
1b	**PMe_3**	**155.0**	**141.4**	**0.23**
1	PMe_3	155.5	141.3	0.23
TS-1	*PMe_3*	*143.9*	*143.1*	*0.01*
2b	**$P(OMe)_3$**	**155.1**	**138.3**	**0.28**
2c	**$P(OMe)_3$**	**151.1**	**149.8**	**0.02**
2d	**$P(OMe)_3$**	**157.0**	**142.0**	**0.25**
2	$P(OMe)_3$	155.5	144.0	0.19
2′[c]	$P(OMe)_3$	157.4	136.3	0.35
2″[c]	$P(OMe)_3$	154.2	139.6	0.24
2‴[c]	$P(OMe)_3$	152.2	146.7	0.09
3	PH_3	151.6	151.6	0.00
TS-3	*PH_3*	*144.2*	*144.2*	*0.00*

[a] Experimental (X-ray) values are given in boldface type, BP86 optimized minima are given in lightface type, and transition states for π−allyl rotation are given in italics. [b] α and β are the two largest angles formed between the metal and any two donor atoms attached to it. [c] Higher energy form.

been calculated by the extended Hückel method.[37a] Very recently, a series of DFT studies on $(\eta^3\text{-}C_3H_5)M(PMe_3)_n(CO)_{3-n}$ (M = Co, Rh, Ir; $n = 0-3$) and other π-allyl complexes has been carried out.[38]

Geometry optimization for the isolated cation $[(\eta^3\text{-}C_3H_5)Ni(PMe_3)_3]^+$ (**1**) started from an approximate *SPY*-5 structure with one apical phosphine but converged qualitatively to the same arrangement as found in the solid for **1a**,**b**. The main quantitative difference of the DFT structure is an overestimation of the Ni−P bond lengths, which is a typical result for the level employed. The pattern of one short and two longer Ni−P distances observed in the solid is also seen in the BP86/AE1 values (2.22, 2.27, and 2.30 Å). According to energy evaluations at the BP86/AE1 level, the fully optimized **1** is, respectively, 4.8 and 5.7 kcal/mol more stable than the cations in the solid-state structures of **1a** and **1b** (after relaxation of the H positions).[39] The dissociation reaction (eq 3) is calculated to be endothermic for

$$[(\eta^3\text{-}C_3H_5)Ni(PMe_3)_3]^+ \rightarrow [(\eta^3\text{-}C_3H_5)Ni(PMe_3)_2]^+ + PMe_3 \quad (3)$$

1 by 5.3 kcal/mol, in accord with the fact that **1a**−**d** are stable and isolable.[40] The computed ^{31}P chemical shifts of **1** are $\delta(P)_{calcd}$ 26, −6, and −25 for P1, P2, and P3, respectively. The similarity of these values[41] to those derived from the ^{31}P CP-MAS spectra ($\delta(P)_{exp}$ 3, −18, and −25 for **1a**) supports the assignment.

From the NMR spectroscopic studies a facile relative rotation of the three PMe_3 ligands versus the π-allyl group was inferred for **1a**−**d**. The transition state **TS-1** for this process in the free cation has been located. Its structure is clearly *SPY*-5, with one longer (2.38 Å) and two short Ni−P bonds (2.23 Å each), the former eclipsing the $C-H_{meso}$ bond of the allyl moiety (i.e., PMe_3 is in an exo position). That **TS-1** is on a minimum energy path to **1** is apparent from the imaginary mode, which describes the turnstile rotation[42] of the Ni(allyl) and $Ni(PMe_3)_3$ groups relative to one other, and this has been proven by explicitly following the intrinsic reaction coordinate.[43] The computed barrier for allyl rotation is only 3.5 kcal/mol, consistent with the fluxional character of **1a**−**d** on the NMR time scale.

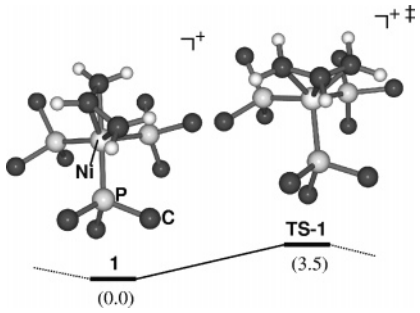

We investigated a possible $\pi-\sigma$ allyl isomerization process for the dynamics of the allyl group, but attempts to locate a σ-allyl isomer were unsuccessful and always afforded the π-allyl minimum **1**. Only by imposing C_s symmetry on the cation could a stationary point corresponding to $[(\eta^1\text{-}C_3H_5)Ni(PMe_3)_3]^+$ (**1′**) be located. This form possesses a near-ideal square-planar arrangement and represents a transition geometry for the $\pi-\sigma-\pi$ allyl rearrangement of **1**.[44] Its energy lies 19.1 kcal/mol above that of the ground-state structure. Thus, according to these calculations it appears that $\pi-\sigma$ allyl isomerization is strongly disfavored with respect to apparent π-allyl rotation, in agreement with the experimental results.

For the pristine cation $[(\eta^3\text{-}C_3H_5)Ni\{P(OMe)_3\}_3]^+$ (**2**) the identification of the global minimum is hampered by the fact that even for a given conformational set of the $P(OMe)_3$ ligands (such as *B*,*B*,*C* and *B*,*C*,*C*) numerous orientations of the OMe substituents are feasible, which are likely to be very close in energy. We optimized a total of four different conformers, chosen according to structural precedence, from the literature and from the present work. As expected, the energy range spanned by these minima is small, amounting to just 1.2 kcal/mol. The most stable form, **2**, was obtained using the coordinates of the cation in solid **2c** as a starting point for the optimization. In **2** the conformational *B*,*B*,*C* pattern of **2c** is retained, with the apical phosphite adopting conformation *C*. While **2c** is clearly *SPY-5* ($\tau = 0.02$), the optimized structure **2** ($\tau = 0.19$) is significantly distorted toward *TBP*-5. Using the ligand conformation observed in $(\eta^3\text{-cyclooctenyl})Co\{P(OMe)_3\}_3$[17c] as a starting point, a second *B*,*B*,*C* minimum (**2‴**) was obtained. The minimum **2‴** is 1.2 kcal/mol higher in energy than **2** and is much closer to an ideal *SPY*-5 arrangement ($\tau = 0.09$) with two short basal (2.17 and 2.19 Å) and one long apical Ni−P

(38) Ariafard, A.; Lin, Z. *Organometallics* **2005**, *24*, 3800 and references therein.

(39) The positions of the H atoms were optimized at the BP86/AE1 level, while all other atoms were fixed at their positions in the solid. This procedure is intended to account for the inherently different nature of equilibrium bond lengths (distances between nuclei) and X-ray-derived separations (distances between electron-density maxima), which are especially disparate when H atoms are involved. Computed energies of so-called H-relaxed geometries have been used to assess experimental, refined structures; see e.g.: Brain, P. T.; Bühl, M.; Fox, M. A.; Greatrex, R.; Hnyk, D.; Nikrahi, A.; Rankin, D. W. H.; Robertson, H. E. *J. Mol. Struct.* **1998**, *445*, 319.

(40) In the gas phase and at room temperature, entropic contributions would also render **1** unstable with respect to PMe_3 loss, due to the increase in particle numbers. In solution, more complicated equilibria have to be considered: in particular, those that involve contact ion pairs with the counterion.

(41) When the H-relaxed cation geometry of **1a** (X-ray) is used as input in the NMR calculation, $\delta(P)$ 20, −26, and −34 are obtained, which are even closer to the observed shifts.

(42) Ugi, I.; Marquarding, D.; Klusacek, H.; Gillespie, P.; Ramirez, F. *Acc. Chem. Res.* **1971**, *4*, 288. Ramirez, F.; Pfohl, S.; Tsolis, E. A.; Pilot, J. F.; Smith, C. P.; Ugi, I.; Marquarding, D.; Gillespie, P.; Hoffmann, P. *Phosphorus Relat. Group V Elem.* **1971**, *1*, 1.

(43) (a) Gonzales, C.; Schlegel, H. B. *J. Chem. Phys.* **1989**, *90*, 2154. (b) Gonzales, C.; Schlegel, H. B. *J. Phys. Chem.* **1990**, *94*, 5523.

(44) Actually, C_s-symmetric **1′** is a second-order saddle point, since there is a second, very small imaginary mode ($6i$ cm^{-1}) in addition to the imaginary frequency of $120i$ cm^{-1} describing the allyl rearrangement. We did not locate the true transition state, since its energy should be very similar to that of **1′**.

Table 7. Summary of the Phase Properties of the [(η^3-C_3H_5)Ni(PR_3)$_3$]Y Complexes 1a−d and 2a−d[a]

	anion	geom	mp/dec pt (°C)	phase transition (°C)	mobility (CP-MAS NMR)[b] phase	P ligands	allyl	anion	plastically cryst phase
1a	OTf	*TBP*-5	122 dec	−		+	−	+	−
1b	PF_6	*TBP*-5	126 dec	40.5	II	+	−	(−)	−
1c	Br	*SPY*-5	138	−18	II	−	n.d.	−	−
					I	+	+ (NQS)	−	−
1d	I	*SPY*-5	145	−55.5	II	−	n.d.	−	−
					I	+	+ (NQS)	−	−
2a	OTf	*TBP*-5	130	−21 (SC: 10−15°)	II	+	n.d.	(+)	−
					I	+	+	+	+
2b	PF_6	*TBP*-5	130	15	III	−	−	−	−
				53 (SC: 70°)	II	(+)	−	−	−
					I	+	+	+	+
2c	Br	*SPY*-5	>110	50	II	−	−	−	−
2d	I	*TBP*-5	>110	68	II	−	−	−	−

[a] Legend: SC, supercooling; n.d., not determined. [b] At 28 °C (301 K) or close to the temperatures of the phase transitions (see text).

bond (2.26 Å). Although **2‴** shows essentially the same structural characteristics as the cation of **2c**, both complexes differ in a number of details, namely in the particular distribution of anti and gauche conformations, in some orientations of the latter, and in some of the rotational angles of the phosphite groups about the Ni−P bonds (Figure S15).

Bracketed in terms of energy by **2** and **2‴**, two minima with *B,C,C* conformation were obtained. One of these, **2″**, resulted from an optimization starting from the cation in **2b**, which preserved the *TBP*-5 arrangement, as reflected in the short−long−long Ni−P distance pattern (2.18, 2.22, and 2.23 Å) and the large value of the angular parameter ($\tau = 0.24$), similar to that in solid **2b** ($\tau = 0.28$). In the second *B,C,C* isomer, **2′**, which was derived from the particular $P(OMe)_3$ conformations in (η^3-benzyl)Co{$P(OMe)_3$}$_3$,[17d] the distortion toward a *TBP*-5 structure is most pronounced ($\tau = 0.35$). **2′** and **2″** show the same distribution of *B* and *C* conformations over the three phosphite sites and differ only in a few points, where an alternate gauche orientation is realized or where gauche and anti orientations are switched (Figure S16). As mentioned above, all four conformers are very close in energy, with the energetic ordering **2** (0.0) < **2′** (0.9) < **2″** (1.1) < **2‴** (1.2) (E_{rel} in kcal/mol given in parentheses). In all, the results indicate that in (π-allyl)Ni{$P(OMe)_3$}$_3$ complexes *B,B,C* and *B,C,C* conformations of the phosphite ligands induce *SPY-5* and *TBP-5* coordination geometries, respectively, irrespective of the finer conformational details. The intrinsic energetic discrimination between the two geometries is small, however, and weak interactions with the anion, for instance, may be decisive for the preference of one geometry over the other.

The structure of the elusive parent cation with three PH_3 ligands, [(η^3-C_3H_5)Ni(PH_3)$_3$]$^+$ (**3**), was also investigated. Start-

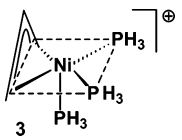

3

ing the optimization from the geometry of **1**, obtained by simply replacing the 9 Me groups by H atoms, resulted in a stationary point that preserves the essential structural features of **1**. However, this structure turns out to be a transition state for rotation of one PH_3 group, **TS-3**. When this imaginary mode was followed, the system collapsed to a C_s-symmetric *SPY*-5 minimum (Ni−P distances 2.02, 2.02, and 2.31 Å), which is merely 1.2 kcal/mol more stable, and which is the only minimum that could be located for **3**.

It thus seems that whereas electronic factors would favor a *SPY*-5 structure for [(η^3-C_3H_5)NiL_3]$^+$ complexes (L = monodentate phosphorus ligand), already a relatively small bulk of the ligands L destabilizes this structure with respect to a more spacious *TBP*-5 structure.

Discussion

We have described the synthesis and structural and dynamic properties of ionic five-coordinate [(η^3-C_3H_5)NiL_3]Y complexes **1a−d** and **2a−d** (L = phosphine, phosphite) in solution and in the solid state. On the basis of the results from DSC, solution and solid-state NMR, and single-crystal and powder X-ray crystallography as well as DFT calculations we are now in a position to draw some general conclusions about the structure and dynamics of the complexes. The findings are summarized in Table 7.

1. *Solid state ^{31}P NMR spectroscopy* served as a powerful tool for *structure determination* of the [(η^3-C_3H_5)Ni(PR_3)$_3$]Y complexes (PR_3 = PMe_3, $P(OMe)_3$). For the complexes with distorted *TBP*-5 geometry **1a**,**b**, **2b-III/-II**, and **2d** the π-allyl ligand occupies an axial and an equatorial site, leaving the other axial site and two equatorial sites for the phosphorus ligands. Because of this position of the allyl group the complexes are necessarily of C_1 symmetry; that is, all three phosphorus ligands and the two termini of the allyl group are each inequivalent. Typically, in the ^{31}P NMR spectra for the axial P1 a pseudo-singlet (or a multiplet) as an unresolved doublet of doublets at low field and for the equatorial P2 and P3 a pair of doublets of doublets at high field are found (Figure 19). This pattern of signals results from a large coupling between the equatorial P2 and P3 and much smaller couplings between these ligands and the axial P1.

For the PMe_3 ligated **1d** with the *SPY*-5 geometry the signal of P2 is shifted to low field close to P1, since both ligands now occupy a similar basal position, whereas the more weakly coordinated apical P3 remains at high field. Similarly, for the $P(OMe)_3$-ligated **2c** the signals of the basal P1 and P2 are likewise close to each other, but the apical P3 has moved substantially to low field. In addition, the large coupling has vanished. As a result, the nearly C_s-symmetrical *SPY*-5 complexes give rise to a pseudo-singlet for the apical P3 and a pair of very close doublets for the basal P1 and P2 (Figure 19; for **1c** an intermediate situation is encountered). The assignment of the structures by solid-state ^{31}P NMR was made mainly on the basis of the couplings. For complexes **1a**,**b** and **2b−d** the structures were determined by solid-state NMR and verified by X-ray structure analysis. It is worth noting that the coordination chemical shifts[45] of the PMe_3 ligands in **1a−d** are quite large

(45) Jolly, P. W.; Mynott, R. *Adv. Organomet. Chem.* **1981**, *19*, 257.

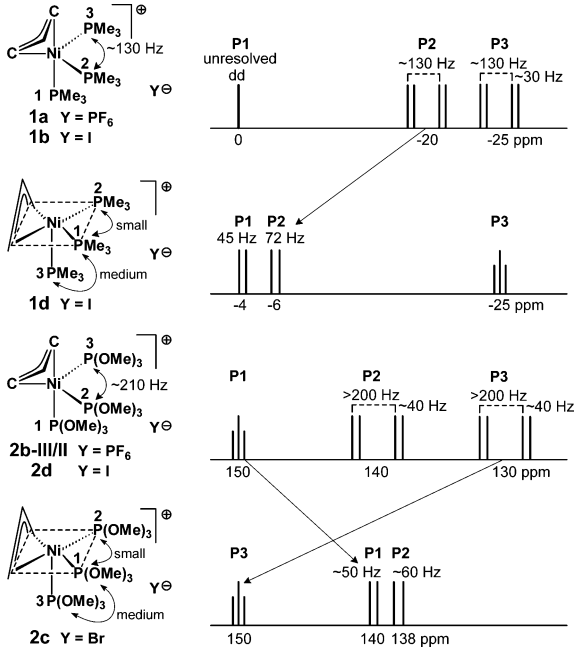

Figure 19. Schematic presentation of the ground-state ^{31}P CP-MAS NMR signal patterns of the $[(\eta^3\text{-}C_3H_5)Ni(PR_3)_3]Y$ complexes **1a**−**d** and **2b**−**d**.

and positive ($\Delta\delta = 35-65$ ppm), whereas the values for the $P(OMe)_3$ ligands in **2a**−**d** are much smaller ($\Delta\delta = +11$ to -16 ppm).

2. The five-coordinate $[(\eta^3\text{-}C_3H_5)Ni(PR_3)_3]Y$ complexes display two *ground-state structures*. On the basis of X-ray structure determinations and the solid-state NMR spectra the structures of the Ni^{II}−allyl complexes **1a**,**b** and **2b**,**d** are best viewed as distorted *TBP*-5. The angular parameter τ, which serves as a simple guide for Berry-type distortions,[25b] lies in the range $0.35 \geq \tau \geq 0.23$ and thus is intermediate between the values expected for the ideal *TBP*-5 ($\tau = 0.67$) and *SPY*-5 ($\tau = 0$) structures. There is generally a good agreement between the experimentally determined and calculated (DFT) geometries **1** and **2**. The computed strictly *SPY*-5 structure of the hypothetical $[(\eta^3\text{-}C_3H_5)Ni(PH_3)_3]^+$ (**3**) suggests that in **1a**,**b** and **2b**,**d** the distortions toward *TBP*-5 arise from repulsive ligand−ligand interactions, rather than from an intrinsic electronic effect of the five-coordinated Ni^{II} center (cf. ref 9c, p 358). However, the observed *SPY*-5 structure of the bromide **2c** in the solid state can be attributed to an interaction of the bromide ion with the OMe substituents of the cation, thereby fixing this geometry. *TBP*-5 structures (as are *SPY*-5 structures) are well-established in Ni^{II} coordination chemistry.[9c] The ease of geometrical distortion in five-coordinate complexes explains the differences in the cation geometries of **1a**,**b** and accounts also for the fact that the cations in **2b**,**d** have a distorted *TBP*-5 geometry, while the cation of **2c** is *SPY*-5.

3. The solid complexes **1b**−**d** and **2a**−**d** are all *polymorphic*. While for the PMe_3 complex **1a** an explicit phase transition was not detected, the derivates **1b**−**d** undergo distinct crystalline−crystalline transitions. According to DSC the energy changes involved are generally small (15−20%) compared to the enthalpy of melting. Although the phosphorus atoms are dynamic for **1a**−**d** at ambient temperature (**1b-II**, **1c-I**, and **1d-I** are present here), the allyl ligands are essentially fixed, as evidenced by their asymmetric structure in the solid-state NMR spectra. The observed relatively slow structural dynamics of the complexes are in accordance with the crystalline nature of the phases.

The $P(OMe)_3$ triflate **2a** separates from solution in the phase **2a-II**. It has been verified by X-ray powder diffractometry that this phase is indeed crystalline. However, neither single-crystal structure analysis nor solid-state NMR allowed an unambiguous assignment of its structure. Although solid-state NMR does not exclude a dynamic structure of **2a-II**, the spectra are in agreement with the presence of a mixture of conformers. According to DSC **2a-II** transforms at −21 °C endothermically into the high-temperature (HT) phase **2a-I**. The phase transition is reversible, but there is a considerable supercooling of 10−15 K, indicating that in order to resume the original structure major structural rearrangement has to take place. Unfortunately, it has not been possible to relate the enthalpy of transition to an enthalpy of melting because of decomposition of the complex, and further investigations of the transition, e.g., by a polarizing microscope, have been hampered by the low transition temperature. For the phase **2a-I** X-ray powder diffractometry reveals the presence of a cubic primitive cell and solid-state NMR indicates highly mobile ions. These results suggest that **2a-I** is a plastically crystalline mesophase.

The various phases and transitions of the $P(OMe)_3/PF_6$ salt **2b** have been studied intensively. Thus, the phase **2b-III**, which crystallizes from THF solution at 0 °C, transforms at 20 °C slowly and reversibly into the likewise crystalline phase **2b-II** ($T_c \approx 15$ °C, eq 1). When either **2b-III** or **2b-II** is heated to 50 °C, it transforms into the plastically crystalline mesophase **2b-I**, as evidenced by DSC, X-ray powder diffractometry, and solid-state NMR. Qualitative inspection of the DSC curve indicates that the transition enthalpy of **2b-II** → **2b-I** is much larger than the diminutive enthalpy of melting. Cooling **2b-I** affords first **2b-II**. The formation of **2b-II** occurs instantaneously under the conditions of solid-state NMR and X-ray powder diffractometry, but it is associated with a >70 K supercooling in DSC. Recovery of **2b-III** from **2b-II** is a relatively slow process and is best achieved at 10 °C, since **2b-II** is metastable below −20 °C.

The halides **2c**,**d** are also polymorphic. Only the crystalline structures stable at ambient temperature have been studied in detail. The nature of the HT phases remains unclear, and no indication was found that they occur as plastically crystalline (PC) mesophases.

4. *Is there evidence for anion mobility?* While solid-state NMR allowed an investigation of the structural dynamics of the cations, the question whether the anions are also mobile is less readily answered. In the ambient-temperature ^{13}C CP-MAS NMR spectra of the triflate complexes **1a** (monoclinic phase) and **2a** (PC phase) the CF_3 signal is of markedly lower intensity than in the corresponding MAS NMR spectra. Therefore, cross-polarization appears ineffective, which can be attributed to the dynamic nature of the CF_3 group. In agreement with this, the CF_3 signal is unchanged in the ^{13}C NQS CP-MAS NMR spectrum when compared to the non-NQS spectrum, similar to the situation expected for a methyl group. It can be assumed that the dynamics of the OTf ligand start by rotation of the CF_3 and possibly also the SO_3 moieties about the central C−S bond. Tumbling of the triflate on its site and even its migration through the lattice represent higher energy processes but have nevertheless been shown to occur in rotator phases. While disorder of the triflate ion in crystal structures is quite often encountered, the dynamics of the triflate anion in LiOTf[46a] and the ionic conductivity of CsOTf[46b] have only been studied very recently.

(46) (a) van Wüllen, L.; Hildebrandt, L.; Jansen, M. *Solid State Ionics* **2005**, *176*, 1449. (b) Hildebrandt, L.; Dinnebier, R.; Jansen, M. *Z. Anorg. Allg. Chem.* **2005**, *631*, 1660.

The PF_6 anion is 6-fold degenerate with respect to its fluorine sites (O_h symmetry). Disorder of the PF_6 anion in crystal structures has frequently been noted,[47] and scattered reports have appeared on a possible motion of the PF_6 anion in solid-state structures.[48,49] Inequivalent ^{19}F chemical shifts have been proposed for a distorted PF_6 ion.[48b] The ^{19}F and ^{31}P NMR spectra of PF_6 ions in intercalated graphites have been described.[50] For the PF_6 anion in **1b** and **2b** the ^{31}P CP-MAS NMR signal shows the expected regular 1:6:15:20:15:6:1 septet with a $J(PF) = 705 \pm 3$ Hz coupling. The septet lines are sharpest for **2b-I** ($\delta(P)$ −144.9; 50 °C), with a half line width for the three inner lines of merely 30 Hz, which comes close to a typical value of 5 Hz for a solution NMR spectrum (−80 °C). There are no visible spinning sidebands of the PF_6 septet in the solid-state NMR spectrum of **2b-I**. From the above there is little doubt that there is substantial rotatory and possibly also diffusional motion of the PF_6 anion in **2b-I**, leading to an isotropic local symmetry of the PF_6 anion. For **2b-II** the chemical shift is unchanged, but for **2b-III** it occurs at lower field ($\delta(P)$ −141.6; 28 °C). For the crystalline phases **1b-II/-I** and **2b-III/-II** there is some variation of the septet half line widths, increasing from 30 to 40 Hz for the central line to >100 Hz for the outer lines, and minor spinning sidebands arise for **1b-II**. It appears as an interesting aspect of the ^{31}P CP-MAS spectra of **2b-III/-II** and **1b-II/-I** that there is altogether relatively little variance in ^{31}P PF_6 signal compared to that of the rotator phase **2b-I**, suggesting that the geometry of the PF_6 anion is also isotropic in most of the crystalline phases. For the crystalline halides **1c**,**d** and **2c**,**d** no indication was obtained for a translational mobility of the halide anions.

A more detailed investigation of anion motion would require the application of more sophisticated NMR techniques (an overview is given in ref 46a), which is beyond the scope of the present study. Rotatory motion, diffusion,[51] and ion conduction[52] are now well-accepted properties for plastically crystalline phases.

5. **2a** and **2b** form *plastically crystalline mesophases*. Plastically crystalline complexes are quite common in organic (e.g., neopentane, adamantane) and inorganic chemistry (e.g., P_4, SF_6, various ammonium salts).[29] In organometallic chemistry plastically crystalline mesophases have been very rarely reported, and examples include certain ferrocene derivatives such as octamethylethynylferrocene,[53] while ferrocene itself is polymorphic.[54] To assign a plastically crystalline state to a phase, various criteria need to be satisfied, and the most important of these are (a) a highly symmetric, mostly cubic structure of the lattice, (b) low entropy of fusion (less than 20 J K^{-1} mol^{-1}), (c) isotropic rotation of the molecules of ions, and (d) optical isotropy, in addition to (e) plastic (soft, waxy) properties.

In the DSC spectra of **2a**,**b** the most prominent features are the endothermic transitions **2a-II** → **2a-I** and **2b-III** → **2b-II** → **2b-I** and the exothermic reverse effects **2a**,**b-I** → **2a**,**b-II** associated with a characteristic supercooling. Since either no melting occurred before decomposition (**2a**) or melting occurred concomitant with decomposition (**2b**), an entropy of fusion for comparison could not be determined. However, the transitions **2a-II** → **2a-I** and **2b-II** → **2b-I** were found to be associated with substantial enthalpy and entropy changes of $\Delta H_{252\ K} = 12.5$ kJ mol^{-1} and $\Delta S_{252\ K} = 49.6$ J K^{-1} mol^{-1} (**2a**) and $\Delta H_{326\ K} = 19.3$ kJ mol^{-1} and $\Delta S_{326\ K} = 59.2$ J K^{-1} mol^{-1} (**2b**), indicating that the formation of phase **I** from a crystalline phase is accompanied with the appearance of significant orientational disorder.

Further evidence for the assignment of phase **I** of **2a** and **2b** as a plastically crystalline phase stems from X-ray powder diffractometry, optical isotropy, solid-state NMR, and its waxy properties. While phase **II** of **2a** and **2b** has been shown to be crystalline, the powder spectra of phase **I** have been indexed for a CsCl-type primitive cubic cell, and this is typical for a rotator phase. In addition, it was shown under a polarizing microscope that, while the crystalline phase **II** of **2a** and **2b** is birefringent, phase **I** is isotropic. Solid-state NMR spectra of **2a-I** and **2b-I** exhibit sharp solution-type ^{13}C and ^{31}P NMR signals for both the allyl ligand and the phosphite ligands and show these ligands to be dynamic. The spectra are in agreement with an isotropic environment around the nuclei, best explained by an isotropic rotation of both cation and anion. On the basis of these results there appears to be little doubt that phase **I** of **2a** and **2b** indeed represents a rotator phase.

The question arises as to *why* **2a** and **2b** form plastically crystalline phases. An overview of the solid-state phase properties of the ionic complexes **1a**−**d** and **2a**−**d** in Table 7 shows that, with the exception of **1a**, all complexes exist in at least two different solid phases. For the LT phases the phosphorus ligands in the cations are either rigidly coordinated or undergo relatively slow dynamics (**1b-II**, **2a-II**, and **2b-II**), and in the cases where the allyl ligands have been studied, they have been found to be nondynamic. In the HT phases dynamics of the phosphorus ligands occur quite easily (e.g., **1c-I**, **1d-I**, **2a-I**, and **2b-I**), whereas significant dynamics of the allyl group have only been observed for **2a-I** and **2b-I**. For these phases an additional mobility of the OTf and PF_6 anions has been shown, and as a result the phases are plastically crystalline. It thus appears that a plastically crystalline phase is encountered for those [(π-allyl)NiL_3]Y complexes for which mobility of all ligands of the cation (and thus the cation as a whole) *and* the anion is possible. Clearly, any interaction between cation and anion will reduce the mobility of the ions and suppress the formation of a plastically crystalline phase.

It appears that for the formation of a plastically crystalline phase in [(π-allyl)NiL_3]Y complexes both cations and anions

(47) (a) Rivera, A. V.; Sheldrick, G. M. *Acta Crystallogr., Sect. B* **1978**, *34*, 1716. (b) Sim, G. A.; Woodhouse, D. I. *Acta Crystallogr., Sect. B* **1979**, *35*, 1477. (c) Heeg, M. J.; Endicott, J. F.; Glick, M. D.; Khalifa, M. A. *Acta Crystallogr., Sect. B* **1982**, *38*, 730. (d) Liu, A. H.; Murray, R. C.; Dewan, J. C.; Santarsiero, B. D.; Schrock, R. R. *J. Am. Chem. Soc.* **1987**, *109*, 4282. (e) Bu, X.; Cisarova, I.; Coppens, P.; Lederle, B.; Naughton, M. J. *Acta Crystallogr., Sect. C* **1992**, *48*, 516. (f) Beissel, T.; Della Vedova, B. S. P. C.; Wieghardt, K.; Boese, R. *Inorg. Chem.* **1990**, *29*, 1736. (g) Clegg, W.; Capdevila, M.; González-Duarte, P.; Sola, J. *Acta Crystallogr., Sect. B* **1996**, *52*, 270.

(48) (a) Albert, S.; Gutowsky, H. S. *J. Chem. Phys.* **1973**, *59*, 3585. Kaliaperumal, R.; Srinivasan, R.; Ramanathan, K. V. *Chem. Phys. Lett.* **1983**, *102*, 29. (b) Ono, H.; Ishimaru, S.; Ikeda, R.; Ishida, H. *Bull. Chem. Soc. Jpn.* **1997**, *70*, 2963.

(49) (a) For a report disproving the anticipated PF_6 rotation, see: McBrierty, V. J.; Douglass, D. C.; Wudl, F.; Aharon-Shalom, E. *Phys. Rev. B* **1982**, *26*, 4805. (b) For exclusion of PF_6 transport in a crystalline polymer electrolyte, see: Gadjourova, Z.; Andreev, Y. G.; Tunstall, D. P.; Bruce, P. G. *Nature* **2001**, *412*, 520.

(50) Miller, G. R.; Resing, H. A.; Vogel, F. L.; Pron, A.; Wu, T. C.; Billaud, D. *J. Phys. Chem.* **1980**, *84*, 3333.

(51) Chezeau, J. M.; Strange, J. H. *Phys. Rep.* **1979**, *53*, 1.

(52) MacFarlane, D. R.; Huang, J.; Forsyth, M. *Nature* **1999**, *402*, 792. MacFarlane, D. R.; Meakin, P.; Sun, J.; Amini, N.; Forsyth, M. *J. Phys. Chem. B* **1999**, *103*, 4164 and references therein.

(53) (a) Daniel, M. F.; Leadbetter, A. J.; Richardson, R. M. *J. Chem. Soc., Faraday Trans. 2* **1981**, *77*, 1851. Sato, K.; Iwai, M.; Sano, H.; Konno, M. *Bull. Chem. Soc. Jpn.* **1984**, *57*, 634. (b) Sato, K.; Katada, M.; Sano, H.; Konno, M. *Bull. Chem. Soc. Jpn.* **1984**, *57*, 2361. (c) Asthalter, T.; Franz, H.; van Bürck, U.; Messel, K.; Schreier, E.; Dinnebier, R. *J. Phys. Chem. Solids* **2003**, *64*, 677.

(54) Toscani, S.; de Oliveira, P.; Céolin, R. *J. Solid State Chem.* **2002**, *164*, 131.

have to contribute to a total entropy of transition of a magnitude of about $\Delta S > 50$ J K^{-1} mol^{-1}. The P(OMe)$_3$ ligands with the flexible OMe substituents provide a greater variety of different conformations, and thus, there is a greater possibility of entropy gain associated with these ligands than for the PMe$_3$ ligands. Similarly, mobile anions such as OTf and PF$_6$ provide a larger entropy contribution than the halides. It appears that the entropy contribution from the P(OMe)$_3$ ligands, but not that of the PMe$_3$ ligands, together with that of the OTf and PF$_6$ anions allows for the formation of a plastically crystalline phase. We will show in a subsequent paper that the more flexible NTf$_2$ anion, which can undergo additional N−SO$_2$ rotations, even confers plastic properties on [(π-allyl)Ni(PMe$_3$)$_3$]Y complexes.[20b]

Conclusions

We have described the preparation and characterization of a series of novel ionic five-coordinate [(η^3-C$_3$H$_5$)NiL$_3$]Y complexes with monodentate donor ligands L and their solid-state properties. Almost all complexes undergo solid−solid phase transitions. While all of the complexes have dynamic structures in solution, most of them display dynamic properties in at least one of the solid phases. We show that turnstile rotation of the three donor ligands is the most likely process, but π-allyl rotation may also occur in the solid state. ($\pi-\sigma$ allyl isomerization is not a relevant dynamic process of the complexes, and this will be demonstrated for cyclic donor ligands in a later paper.)

The counteranion Y has a strong influence on the structure (*TBP*-5 vs *SPY*-5), phase transitions, and dynamic properties of the complexes, even though cations and anions are usually well-separated. So far, we have described plastically crystalline mesophases for P(OMe)$_3$-ligated Ni−π-allyl complexes with *TBP*-5 ground-state geometries having OTf and PF$_6$ counterions. In the mesophases, the combined turnstile rotation of the phosphorus ligands and π-allyl rotation appears to result from an interchange of all ligands of the formally five-coordinate cations and thus an apparent tumbling of the whole cations on their site in the lattice. Concomitant anion dynamics appear to be necessary for the occurrence of the mesophase for the ionic complexes.

Preliminary results indicate that the neutral (η^3-C$_3$H$_5$)M-{P(OMe)$_3$}$_3$ (M = Co, Rh, Ir) complexes undergo similar structural dynamics in the solid state. Whether this is indeed the case and whether the dynamics are associated with the formation of a mesophase are presently under investigation.

Experimental Section

All manipulations were carried out under argon using Schlenk-type glassware. Solvents were dried prior to use by distillation from NaAlEt$_4$ or P$_4$O$_{10}$. {(η^3-C$_3$H$_5$)NiX}$_2$ (X = Cl, Br, I)[4] were prepared according to the literature. Microanalyses were performed by the Mikroanalytisches Labor Kolbe (Mülheim, Germany). EI mass spectra were recorded at 70 eV; EI and ESI+ mass spectra refer to ^{35}Cl, ^{58}Ni, and ^{79}Br. Solution ^{1}H NMR spectra were measured at 300 MHz, ^{13}C NMR spectra at 75.5 MHz (both relative to TMS), and ^{31}P NMR spectra at 121.5 MHz (relative to external 85% aqueous H$_3$PO$_4$) on Bruker AMX-300 and DPX-300 instruments. Solid-state ^{13}C CP-MAS NMR spectra were recorded on a Bruker MSL-300 spectrometer, equipped with a double-bearing probe and a Bruker B-VT 1000 temperature control unit. The ZrO$_2$ rotor (7 mm internal diameter) was charged with the complex under argon and sealed by a Kel-F inset. Optimal contact time for ^{13}C CP was 2−3 ms and for ^{31}P CP ca. 2 ms. The spinning rate was between 2 and 5 kHz. The external standard for ^{13}C NMR was adamantane (δ(CH$_2$) 38.40, relative to TMS) and that for ^{31}P NMR solid NaH$_2$PO$_4$ (δ(P) 0.314, relative to 85% H$_3$PO$_4$(aq)). Temperature calibration of the Bruker MAS 7BL probe was performed according to the literature.[55] DSC spectra were recorded with the Mettler-Toledo TA8000 thermal analysis system having a DSC820 measuring module.

X-ray Powder Diffraction Studies on 1b−d and 2a,b. For the in situ X-ray powder diffraction experiments, the samples were sealed in glass capillaries of 0.5 mm diameter. The measurements were performed on a Stoe STADI P transmission diffractometer, equipped with a primary Ge(111) monochromator and a linear position-sensitive detector. For cooling and heating of the samples, a Cryostream Plus system (Oxford Cryosystems, 700 series) was used. The system allows temperature control between 80 and 500 K with a temperature stability of 0.1 K. The wavelength used was λ(Cu Kα_1) = 1.540 56 Å. Powder diffraction data were collected below and above the phase transition temperatures determined by DSC. Full powder patterns were taken from 7 to 40° in 2θ in steps of 0.01° for 1080 s at each step. The long counting times were employed to improve the counting statistics of the position-sensitive detector. For a correct determination of lattice parameters a potential 2θ shift due to instrumental and sample contributions usually has to be corrected by adding an internal standard of well-known peak positions. Since no internal standard was added for this work, the observed lattice parameters represent no exact values. The indexing procedure and the Pawley refinements were performed by using the program DASH 2.2.[56]

(η^3-C$_3$H$_5$)Ni{P(OMe)$_3$}$_2$Br. A solution of {(η^3-C$_3$H$_5$)NiBr}$_2$ (359 mg, 2.00 mmol of Ni) in 30 mL of diethyl ether was combined with P(OMe)$_3$ (496 mg, 4.00 mmol) at −20 °C. Slow cooling to −60 °C gave large red-brown needles, which were washed with some cold diethyl ether and dried under vacuum at −30 °C: yield 660 mg (77%); dec pt ≥20 °C. ESI+ MS (CH$_2$Cl$_2$): *m*/*e* (%) 347 ([M − Br]$^+$, 100). ^{1}H NMR (−30 °C): δ 5.00 (1H, meso), 3.97 (2H, syn), 3.27 (2H, anti), allyl; 3.65 (m, 18H), P(OMe)$_3$. ^{13}C NMR (−30 °C): δ 104.1 (1C), 64.9 ("t", 2C), allyl; 52.3 (s, 6C), P(OMe)$_3$. ^{31}P NMR (−30 °C): δ 143.2. Anal. Calcd for C$_9$H$_{23}$BrNiO$_6$P$_2$ (427.8): C, 25.27; H, 5.42; Br, 18.68; Ni, 13.72; O, 22.44; P, 14.48. Found: C, 25.45; H, 5.48; Ni, 13.93; P, 14.71.

[(η^3-C$_3$H$_5$)Ni{P(OMe)$_3$}$_2$]PF$_6$. A solution of (η^3-C$_3$H$_5$)Ni-{P(OMe)$_3$}$_2$Br (428 mg, 1.00 mmol) in 10 mL of CH$_2$Cl$_2$ was stirred with TlPF$_6$ (380 mg, 1.08 mmol) at −25 °C for 1 h. After removal of the precipitated TlBr, the resulting yellow-orange solution was freed from the solvent under vacuum and the residue was dissolved in 5 mL of THF. Cooling the solution to −60 °C gave yellow-orange crystals, which were washed with cold ether and dried under vacuum (−25 °C): yield 400 mg (81%); mp 42 °C (DSC). ESI+ MS (CH$_2$Cl$_2$): *m*/*e* (%) 347 ([M − PF$_6$]$^+$, 100). ESI− MS (CH$_2$Cl$_2$): *m*/*e* (%) 145 ([PF$_6$]$^+$, 100). ^{1}H NMR (−80 °C): δ 5.39 (1H, meso), 4.53 (2H, syn), 2.87 (2H, anti), allyl; 3.65 (m, 18H), P(OMe)$_3$. ^{13}C NMR (−80 °C): δ 118.6 ("t", 1C), 71.1 ("t", 2C), allyl; 52.5 ("t", 6C), P(OMe)$_3$. ^{31}P NMR (−80 °C): δ 134.4. Note that the chemical shifts differ markedly from those of the bromide. Anal. Calcd for C$_9$H$_{23}$NiO$_6$P$_2$·PF$_6$ (492.9): C, 21.93; H, 4.70; F, 23.13; Ni, 11.91; O, 19.48; P, 18.85. Found: Ni, 11.28; P, 17.84. The sample contained a small amount of THF (NMR).

[(η^3-C$_3$H$_5$)Ni(PMe$_3$)$_3$]CF$_3$SO$_3$ (1a). A solution of {(η^3-C$_3$H$_5$)-NiBr}$_2$ (359 mg, 2.00 mmol of Ni) in 20 mL of diethyl ether was treated with PMe$_3$ (463 mg, 6.10 mmol) and a solution of TlOTf (707 mg, 2.00 mmol) in 10 mL of THF at ambient temperature. The mixture was stirred for 30 min, 10 mL of CH$_2$Cl$_2$ was added, and the precipitated TlBr was removed by filtration. Cooling to −78 °C gave red cubes, which were washed with cold ether and dried under vacuum (20 °C): yield 620 mg (65%); mp >122 °C

(55) (a) Haw, J. F.; Crook, R. A.; Crosby, R. C. *J. Magn. Reson.* **1986**, *66*, 551. (b) Aliev, A. E.; Harris, K. D. M. *Magn. Reson. Chem.* **1994**, *32*, 366.

(56) DASH 2.2 2003; CCDC, Cambridge, U.K.

dec. EI MS (135 °C): *m/e* (%) 324 ([(η^3-C_3H_5)Ni(PMe_3)OTf]$^+$, 5). ESI+ MS (CH_2Cl_2): *m/e* (%) 251 ([(η^3-C_3H_5)Ni(PMe_3)$_2$]$^+$, 100), 175 ([(η^3-C_3H_5)Ni(PMe_3)]$^+$, 40). Solution NMR data are given in Table 2. Anal. Calcd for $C_{13}H_{32}F_3NiO_3P_3S$ (477.1): C, 32.73; H, 6.76; F, 11.95; O, 10.06; Ni, 12.30; P, 19.48; S, 6.72. Found: C, 32.46; H, 6.81; Ni, 12.35; P, 19.53; S, 6.70.

[(η^3-C_3H_5)Ni(PMe_3)$_3$]PF_6 (1b). A solution of {(η^3-C_3H_5)NiBr}$_2$ (359 mg, 2.00 mmol of Ni) and PMe_3 (463 mg, 6.1 mmol) in 5 mL of CH_2Cl_2 was combined with $TlPF_6$ (699 mg, 2.00 mmol) suspended in 5 mL of CH_2Cl_2 (20 °C). The mixture was stirrred for 1 h. After filtration from TlBr the solution was concentrated under vacuum to about 5 mL and an equal volume of diethyl ether was added. Cooling to −30 and −60 °C gave small orange-brown crystals: yield 380 mg (40%); mp >130 °C dec. ESI+ MS (CH_2Cl_2): *m/e* (%) 251 ([(η^3-C_3H_5)Ni(PMe_3)$_2$]$^+$, 100), 175 ([(η^3-C_3H_5)Ni(PMe_3)]$^+$, 30). Anal. Calcd for $C_{12}H_{32}F_6NiP_4$ (473.0): C, 30.47; H, 6.82; F, 24.10; Ni, 12.41; P, 26.20. Found: C, 30.35; H, 6.85; Ni, 12.59; P, 26.14.

[(η^3-C_3H_5)Ni(PMe_3)$_3$]Br (1c). THF solutions (each 10 mL) of {(η^3-C_3H_5)NiBr}$_2$ (180 mg, 1.00 mmol of Ni) and PMe_3 (230 mg, 3.03 mmol) were combined at ambient temperature. Immediately a red microcrystalline precipitate was formed, which was isolated by filtration, washed with some THF, and dried under vacuum: yield 320 mg (78%); mp >130 °C dec. IR (KBr): 3061 cm^{-1} (HC═). ESI+ MS (CH_2Cl_2): *m/e* (%) 251 ([(η^3-C_3H_5)Ni(PMe_3)$_2$]$^+$, 100). Anal. Calcd for $C_{12}H_{32}BrNiP_3$ (407.9): C, 35.34; H, 7.91; Br, 19.59; Ni, 14.39; P, 22.78. Found: C, 35.45; H, 7.77; Ni, 14.56; P, 22.80.

[(η^3-C_3H_5)Ni(PMe_3)$_3$]I (1d). Synthesis was as for **1c** but started from {(η^3-C_3H_5)NiI}$_2$ (227 mg, 1.00 mmol of Ni). A rust-colored microcrystalline precipitate was obtained: yield 330 mg (73%); mp ˜140 °C dec; $C_{12}H_{32}INiP_3$ (454.9). No elemental analysis was performed.

[(η^3-C_3H_5)Ni{$P(OMe)_3$}$_3$]CF_3SO_3 (2a). A solution of {(η^3-C_3H_5)-NiBr}$_2$ (359 mg, 2.00 mmol of Ni) in 10 mL of CH_2Cl_2 was reacted with $P(OMe)_3$ (750 mg, 6.04 mmol) at −20 °C. After addition of an excess of TlOTf (740 mg, 2.1 mmol) the mixture was stirrred for 30 min. The precipitated yellow TlBr was removed by filtration, the solvent was evaporated, and the residue was redissolved in 8 mL of THF to give an orange solution. Orange-red crystals separated at −60 °C, which were washed with cold ether: yield 1.12 g (90%); mp 135 °C dec. ESI+ MS (CH_2Cl_2): *m/e* (%) 347 ([(η^3-C_3H_5)Ni{$P(OMe)_3$}$_2$]$^+$, 100), 223 ([(η^3-C_3H_5)Ni{$P(OMe)_3$}]$^+$, 75). Solution NMR data are given in Table 2. Anal. Calcd for $C_{13}H_{32}F_3NiO_{12}P_3S$ (621.1): C, 25.14; H, 5.19; F, 9.18; Ni, 9.45; O, 30.91; P, 14.96; S, 5.16. Found: C, 25.50; H, 4.92; Ni, 9.56; P, 15.16.

[(η^3-C_3H_5)Ni{$P(OMe)_3$}$_3$]PF_6 (2b). A solution of {(η^3-C_3H_5)-NiBr}$_2$ (180 mg, 1.00 mmol of Ni) in 10 mL of CH_2Cl_2 was reacted with $P(OMe)_3$ (380 mg, 3.06 mmol) and an excess of suspended $TlPF_6$ (365 mg, 1.05 mol) by stirring the mixture for about 30 min at −20 °C. After removal of the precipitated TlBr the resulting orange solution was concentrated to a volume of about 5 mL and small portions of diethyl ether (total of about 3 mL) were added without precipitating the product. Cooling below −20 °C gave fine orange columns, which were washed with cold ether and dried under vacuum: yield 430 mg (70%); mp >120 °C dec. ESI+ MS (CH_2Cl_2): *m/e* (%) 347 ([(η^3-C_3H_5)Ni{$P(OMe)_3$}$_2$]$^+$, 100), 223 ([(η^3-C_3H_5)Ni{$P(OMe)_3$}]$^+$, 50). Anal. Calcd for $C_{12}H_{32}F_6NiO_9P_4$ (617.0): C, 23.36; H, 5.23; F, 18.48; Ni, 9.51; O, 23.34; P, 20.08. Found: C, 23.41; H, 5.31; Ni, 9.62; P, 20.14.

[(η^3-C_3H_5)Ni{$P(OMe)_3$}$_3$]Br (2c). A solution of {(η^3-C_3H_5)-NiBr}$_2$ (180 mg, 1.00 mmol of Ni) in 25 mL of diethyl ether was combined with $P(OMe)_3$ (380 mg, 3.06 mmol) at −20 °C. Slow cooling to −60 °C gave large orange-red cubes, which were washed with cold ether and dried under vacuum at −30 °C: yield 430 mg (78%); mp >60 °C dec. ESI+ MS (CH_2Cl_2): *m/e* (%) 347 ([(η^3-C_3H_5)Ni{$P(OMe)_3$}$_2$]$^+$, 100), 223 ([(η^3-C_3H_5)Ni{$P(OMe)_3$}]$^+$, 10). Anal. Calcd for $C_{12}H_{32}BrNiO_9P_3$ (551.9): C, 26.12; H, 5.84; Br, 14.48; Ni, 10.63; O, 26.09; P, 16.84. Found: C, 25.59; H, 5.81; Ni, 10.65; P, 17.11.

[(η^3-C_3H_5)Ni{$P(OMe)_3$}$_3$]I (2d). A solution of {(η^3-C_3H_5)NiI}$_2$ (554 mg, 2.00 mmol of Ni) in a mixture of 3 mL of CH_2Cl_2 and an equal volume of diethyl ether was combined with $P(OMe)_3$ (750 mg, 6.04 mmol) at −20 °C. More diethyl ether was added dropwise until the solution became turbid. Slow cooling to −60 °C gave orange-red crystals, which were isolated as described above: yield 875 mg (73%); mp >80 °C dec. EI-MS (30 °C): *m/e* (%) 350 ([(η^3-C_3H_5)Ni$P(OMe)_3$I]$^+$, 20). ESI+ MS (CH_2Cl_2): *m/e* (%) 347 ([(η^3-C_3H_5)Ni{$P(OMe)_3$}$_2$]$^+$, 100), 223 ([(η^3-C_3H_5)Ni{$P(OMe)_3$}]$^+$, 20). Anal. Calcd for $C_{12}H_{32}INiO_9P_3$ (598.9): C, 24.07; H, 5.39; I, 21.19; Ni, 9.80; O, 24.04; P, 15.52. Found: C, 23.60; H, 5.20; Ni, 9.57; P, 15.08.

Computational Details. Geometries were fully optimized at the BP86/AE1 level, i.e., employing the gradient-corrected exchange and correlation functionals of Becke[57] and Perdew,[58] respectively, together with a fine integration grid (75 radial shells with 302 angular points per shell), the augmented Wachters basis[59] on Ni (8s7p4d), and the 6-31G* basis[60] on all other elements. This and comparable DFT levels have proven quite successful for transition-metal compounds and are well-suited for the description of structures, energies, barriers, etc.[61] The nature of the stationary points was verified by computations of the harmonic frequencies at that level. Transition states were characterized by a single imaginary frequency, and visual inspection of the corresponding vibrational modes ensured that the desired minima are connected. The computed harmonic frequencies were used unscaled to evaluate zero-point energies. In addition, single-point energy calculations were performed for the BP86/AE1 geometries employing basis II′, i.e., the augmented Wachters basis on Ni, double-ζ basis on H,[62] and the IGLO-basis II[62] (which is of polarized triple-ζ quality) on the remaining atoms, together with the B3LYP functional, the latter according to Becke (hybrid)[63] and Lee, Yang, and Parr.[64] All computations employed the Gaussian 98 program package.[65] Unless otherwise noted, energies are reported using these B3LYP/II′ energies and include the BP86/AE1 zero-point energies.

Magnetic shieldings σ have been evaluated at the B3LYP/II′ level for the optimized geometries, using a recent implementation of the GIAO (gauge-including atomic orbitals)-DFT method.[66] This particular combination of methods has been employed successfully for chemical-shift computations of transition-metal complexes.[67] ^{31}P chemical shifts have been calculated relative to free PMe_3, for

(57) Becke, A. D. *Phys. Rev. A* **1988**, *38*, 3098.
(58) (a) Perdew, J. P. *Phys. Rev. B* **1986**, *33*, 8822. (b) Perdew, J. P. *Phys. Rev. B* **1986**, *34*, 7406.
(59) (a) Wachters, A. J. H. *J. Chem. Phys.* **1970**, *52*, 1033. (b) Hay, P. J. *J. Chem. Phys.* **1977**, *66*, 4377.
(60) (a) Hehre, W. J.; Ditchfield, R.; Pople, J. A. *J. Chem. Phys.* **1972**, *56*, 2257. (b) Hariharan, P. C.; Pople, J. A. *Theor. Chim. Acta* **1973**, *28*, 213.
(61) For instance, see: Koch, W.; Holthausen, M. C. *A Chemist's Guide to Density Functional Theory;* Wiley-VCH: Weinheim, Germany, 2000; and extensive bibliography therein.
(62) For a description of these basis sets, see: Kutzelnigg, W.; Fleischer, U.; Schindler, M. In *NMR Basic Principles and Progress;* Springer: Berlin, Germany, 1990; Vol. 23, pp 165−262.
(63) Becke, A. D. *J. Chem. Phys.* **1993**, *98*, 5648.
(64) Lee, C.; Yang, W.; Parr, R. G. *Phys. Rev. B* **1988**, *37*, 785.
(65) Frisch, M. J. et al. *Gaussian 98*; Gaussian, Inc., Pittsburgh, PA, 1998.
(66) Cheeseman, J. R.; Trucks, G. W.; Keith, T. A.; Frisch, M. J. *J. Chem. Phys.* **1996**, *104*, 5497.
(67) (a) This is true in particular for the δ(metal) values; for the ligand shifts, other DFT variants would also be appropriate. See for instance: Bühl, M.; Kaupp, M.; Malkin, V. G.; Malkina, O. L. *J. Comput. Chem.* **1999**, *20*, 91. (b) For an application of this particular DFT combination to ligand shifts, see: Bühl, M.; Sassmannshausen, J. *Dalton Trans.* **2001**, 79.

which a σ value of 356.2 ppm is obtained at the same level, and have been converted to the usual δ scale using the experimental solution chemical shift of PMe_3: $\delta(P)$ −61.4.

Acknowledgment. We thank Mrs. Waltraud Ben Mustapha for diligent experimental assistance and Dr. G. W. H. Höhne for valuable comments on the DSC spectra. This work is dedicated to Professor Günther Wilke in recognition of his seminal studies in metal-allyl chemistry.

Supporting Information Available: Complete ref 64, Figures S1−S16, and CIF files giving crystallographic data for **1a**,**b** and **2b**−**d**. This material is available free of charge via the Internet at http://pubs.acs.org.

OM0601807